

CFD STUDY OF SLOSHING IN RECTUNGLAR TANK

AMIT KUMAR BAGHEL

A Dissertation Submitted to
Indian Institute of Technology Hyderabad
In Partial Fulfillment of the Requirements for
The Degree of Master of Technology



भारतीय प्रौद्योगिकी संस्थान हैदराबाद
Indian Institute of Technology Hyderabad

Department of Mechanical Engineering

July 2013

Declaration

I declare that this written submission represents my ideas in my own words and where others ideas or words have been included, I have adequately cited and referenced the original sources. I also declare that I have adhered to all principles of academic honesty and integrity and have not misrepresented or fabricated or falsified any idea/data/fact/source in my submission. I understand that any violation of the above will be a cause for disciplinary action by the Institute and can also evoke penal action from the sources that have thus not been properly cited, or from whom proper permission has not been taken when needed.

Amit

(Signature)

Amit Kumar Baghel

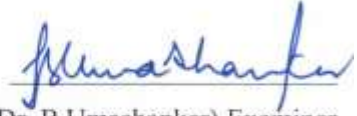
(Amit Kumar Baghel)

ME11M01

(Roll No)

Approval Sheet

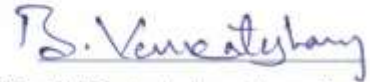
This thesis entitled “CFD study of sloshing in rectangular tank” by “Amit Kumar Baghel” is approved for the degree of Master of Technology from IIT Hyderabad.



(Dr. B. Umashankar) Examiner

Dept of Civil Engineering,

IITH



(Dr. B. Venkatesham) Examiner

Dept. of Mechanical Engineering,

IITH



(Dr. Raja Banerjee) Adviser

Dept. of Mechanical Engineering,

IITH

Acknowledgement

First and foremost, I would like to thank my research advisor, Dr Raja Banerjee, for his advice and support during the work. He gave me the freedom to pursue my ideas and work at my own pace, and was always available to discuss various problems on the way. I also want to thanks Dr. B. Venkatesham for clearing my doubt in the experimental set up .His suggestions were very usefull.

I would like to express my sincere thanks to Mercedes-Benz company to provide financial support for my project.A special thanks to our project staff Mr Sachin and Mr Aranay who helped to provide experimental result. I would like to express my sincere thanks to support people of cd adapco specially Mr. Srikanth, Mr Srikar,Mr Jagan Mohan,Mr Magesh who helped to learning STARCCM+ software. I want to thanks Research scholar Mr Sumer for clearing my concept.

I also want to thanks my all classmates Nitish, Patel, Mudassar, Nikhil, Pankaj, Santosh and all my juniors of Thermo-Fluid Anil, Ashwani, Ali, Satish, Nikhil, Shashi, Vaisakhan, Varun, Vatsalya. I want to thanks my B.Tech friends of IIT Hyderabad specially KVS Pawan, Ajay,Mukesh,Sharath, Uday Kumar,Navya Tej for sharing their knowledge. I would like to thanks my lab mates Mr Madhu, Ms Nagalakshmi for providing support during my thesis work.

At the end i am thank full to my parents for continuous support and motivation in my two years in IIT Hyderabad. I am thank full to my elder sister Mrunalini for her support and her blesses .I would like to thanks to my childhood friends Jitendra and Bittu for there continuous support during my M.Tech.I would like to thanks Mr G.K. Sahu for excellent guidance during my BE,without his guidance I could not get opportunity to do M.Tech in IIT Hyderabad. I am thankfull to God who always helped me during my tough time in IIT Hyderabad.

Dedicated to my parents

Abstract

Due to vehicle acceleration or deceleration, fuel inside and automotive fuel is subjected to inertial acceleration or deceleration, which causes to slosh thereby generating sloshing noise. In the premium segment of cars this noise is considered to be an irritant to passenger because of low background noise. As part of an ongoing research project at IIT Hyderabad, both experimental and CFD studies are performed to understand and predict this sloshing noise. As part of my MTech thesis, two-phase, multi-dimensional and time-accurate CFD simulations were performed to simulate liquid sloshing for a rectangular tank. Commercial CFD solver STAR CCM+ was used to perform the CFD simulations. VOF multiphase model was used to track the evolution of the liquid surface for different acceleration values. Images from high speed video camera was used to validate the current CFD simulations. Parametric studies on the effect of acceleration amplitude, frequency and fill level on liquid sloshing behavior was studied.

Nomenclature

α	Characteristic function
u_i	Velocity in x direction
u_j	Velocity in y direction
μ	Dynamic Viscosity
ν	Kinematic viscosity
p	Pressure
t	Time
b_i	Body force
x	Displacement
A	Amplitude
ω	Angular frequency
F	Acceleration
a	Tank length
h	Fluid height
L	Characteristic length
U_i	Mean velocity
u_i'	Fluctuating component
τ_{ij}	Reynolds shear stress
k	Turbulence kinetic energy
ε	Turbulence dissipation rate
δ_{ij}	Chronicle delta
μ_t	Turbulence viscosity
C	Velocity
Δx	Grid
Δt	Time step

Contents

Declaration.....	ii
Approval Sheet.....	iii
Acknowledgement.....	iv
Abstract	vi
Nomenclature	vii
1.Introduction.....	1
1.1 Slosh noise.....	3
1.1.1 Hit noise.....	3
1.1.2 Splashnoise.....	4
1.1.3 Clonk noise.....	4
1.2 Litreture review.....	4
1.3 Objective.....	5
1.4 Outline.....	5
2. Mathematical Model.....	6
2.1 Governing equations.....	6
2.2 Modeling time.....	8
2.3 Fluid property	11
2.4 Boundry condition	12
2.5 Turbulence modeling.....	12
2.6 Wall funcion.....	14
3. Computational grid and solution procedure.....	15
3.1 Computational Grid.....	15
3.1.1 Classification of grid	16
3.2 Test problem computational grid.....	20
3.3 Numerical solution procedure	24
3.4 Experiment setup	25

4. Results and discussion	26
4.1 Grid independence.....	26
4.2 Time step.....	28
4.3 Validation.....	30
4.4 Viscous effect.....	34
4.5 Parametric study.....	35
4.5.1 Effect of fill level.....	35
4.5.2 Effect of time period.....	38
4.5.3 Effect of amplitude.....	39
4.7 Validation from experiments.....	40
5. Conclusion	43
5.1 Conclusion from simulation.....	43
5.1.1 CFD grid.....	43
5.1.2 Time step.....	43
5.1.3 Laminar or turbulence flow.....	43
5.1.4 2D or 3D.....	43
5.2 Parametric study conclusion.....	44
5.2.1 Effect of fill ratio.....	44
5.2.2 Effect of time period.....	44
5.2.3 Effect of amplitude.....	44
5.3 Conclusion from CFD and experiments.....	44
5.4 Future work.....	45
References	46

Chapter 1

Introduction

Liquid sloshing occurs when a partially filled tank is subjected to an external force [1]. Due to sloshing, the liquid free surface oscillates from one side of the tank to the other. Sloshing phenomena is associated with all types of liquid storage; for ex. automotive fuel tank, LNG carriers spacecraft, etc. Sloshing phenomena depends on of tank geometry fill level and excitation frequency. If the tank is completely filled with liquid, liquid behaves like a solid body and its motion follows that of the container. If excitation frequency is close to natural frequency, then it can cause instability of the vehicle. During sloshing, the free surface can experience different types of motion including simple planar, non-planar, symmetric, asymmetric quasi periodic and chaotic[2] .

Sloshing causes generation of dynamic load and slosh noise. When an automotive vehicle accelerates or decelerates, fuel inside an automotive fuel tank sloshes and generates slosh noise. Slosh noise is perceived by passengers in the vehicle which can reduce their comfort level. Sloshing may also sometime damage the vehicle chassis. So it is necessary to design an automotive fuel tank which can minimize slosh noise. Automotive fuel tanks can be categorized on the basis of their chamber design. In a single tank, there is only one chamber. However, in a saddle tank, there are two chambers with two different lengths. Hence its sloshing behavior is different from that of the single chamber fuel tank. Fig 1.1 shows both the fuel tanks.



Figure1.1 : Single chamber tank (left) and saddle tank (Right) [13]

Slosh noise is a complex mechanism. Vibrations are transferred through the tank structure. As shown in Figure 1.2 passenger perceive noise as airborne noise and structure borne noise. In air borne noise the “sound source “ is a source of noise. Air borne noise propagates through air, hole across the surface of structure. In structure borne noise “sound source” is source of vibration of noise. Vibration propagates through car structure to walls of passenger area. Surfaces radiate sound into the passenger compartment. The acoustic model of the fuel tank is shown below

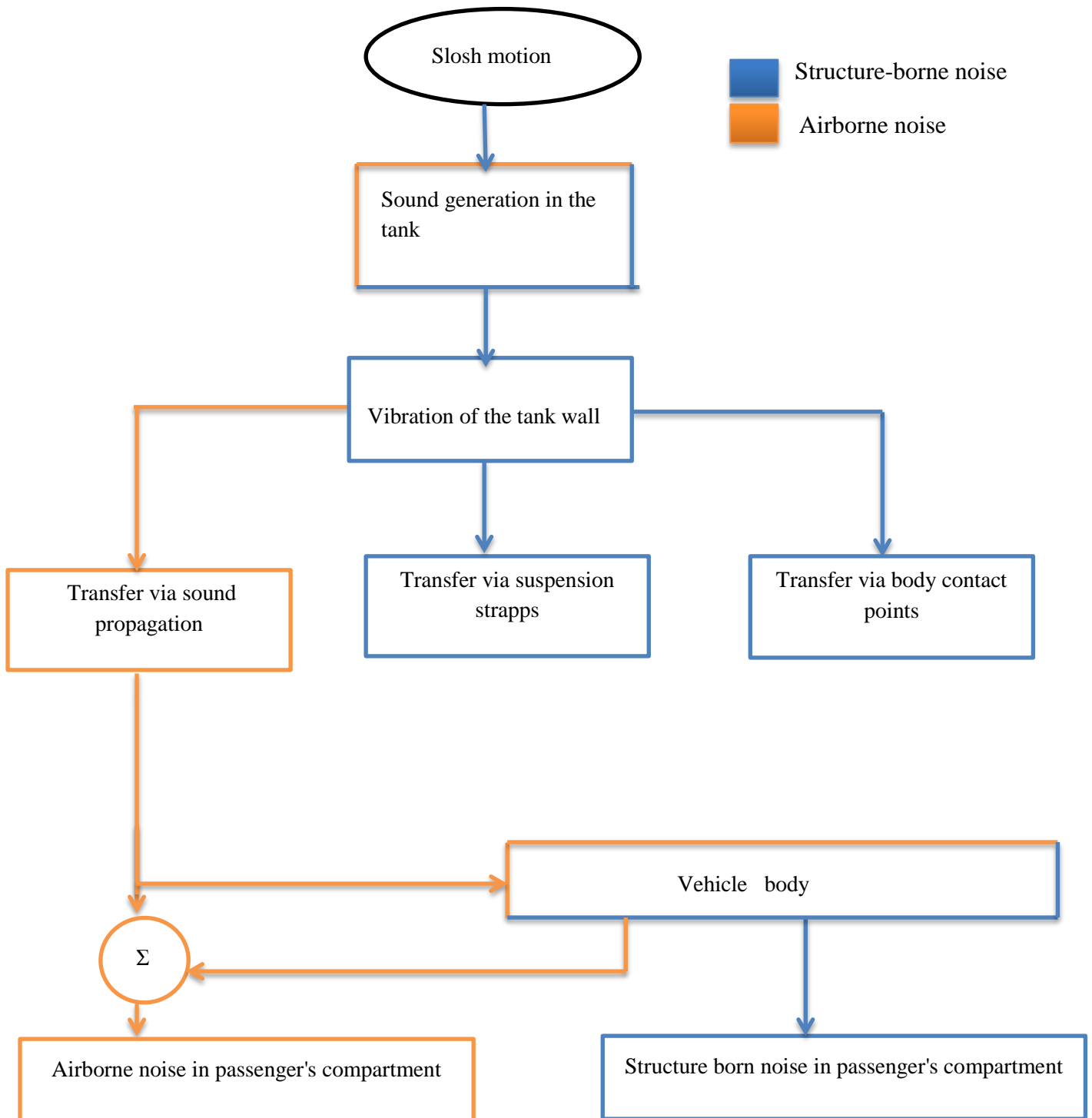


Fig 1.2 : Model of the acoustic system [13]

1.1 Slosh noise

Sloshing causes generation of slosh noise. Slosh noise classified as hit noise, splash noise and clonk noise.

1.1.1 Hit noise

Hit noise is generated due to liquid hitting with interior of wall. Sound Intensity of hit noise is high because of large mechanical interaction of the fluid with the wall. The characteristic of sound are depend on acoustic property of wall. Its frequency is in the range of 0.2 to 2 kHz. Red line shows the generation of sound.

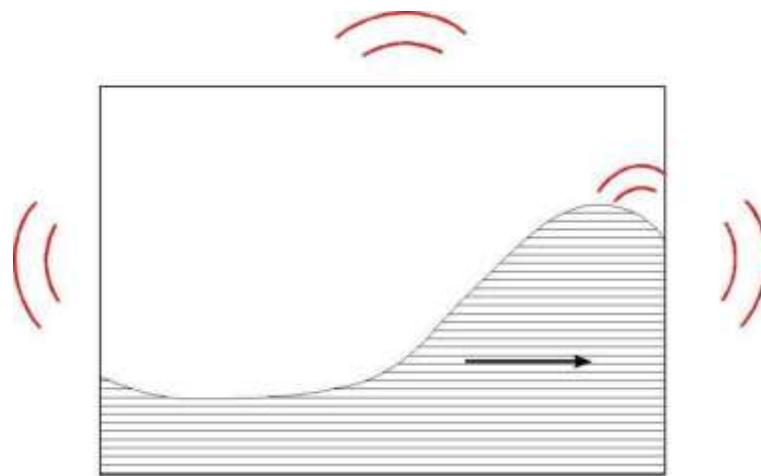


Figure 1.3: Hit noise [13]

1.1.2 Splash noise

Splash noise is generated due liquid hitting with liquid. Its frequency in the range of 0.5 -10kHz.

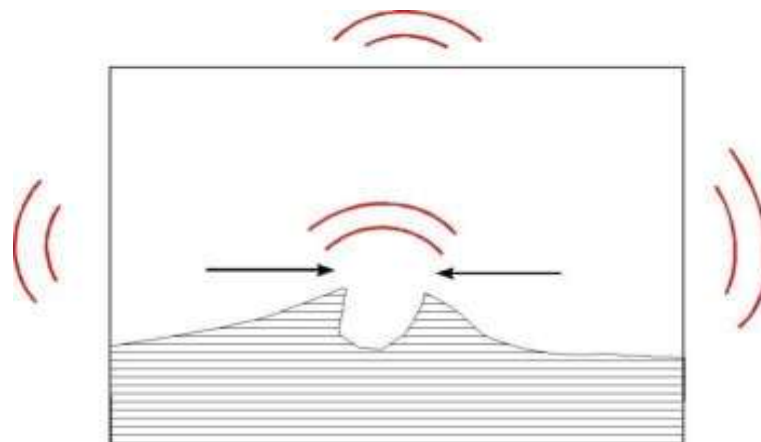


Figure 1.4 : Splash noise[13]

1.1.3 Clonk noise

Clonk noise is generated when air is abruptly compressed by the sloshing liquid. It produces noise characteristic that is similar to gear clonk sound. Its intensity is lowest among the three types of and is in the range of 150- 500Hz. It is generated for a very short time.

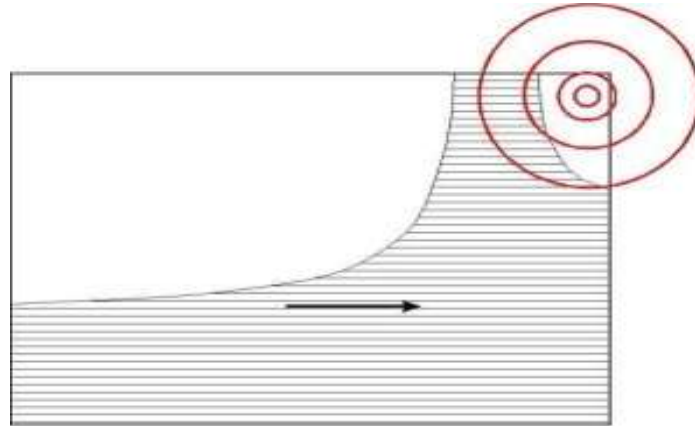


Figure1.5 : Clonk noise [13]

1.2 Literature review

Sloshing has been a broad area from research from many decades. Harald Olsen [1] defined broad meaning of sloshing. Abramson [4] used linear wave theory for used a linear theory to simulate small amplitude sloshing in a container. Khezzi et al. [5] studied sloshing in rectangular tank subjected to impulsive force and found that flow visualization of experimental and simulation shows good results. Similar study was conducted by Rezaei et al. [6] on a rectangular tank and developed a computer code for sloshing and result from Hintasu et al. [8] was used to validate their result. It is observed the dynamics of the flow is well predicted as the visualizations show good agreement with numerical model for some distinct flow features, such as the traveling wave inside the tank and the impact at the end wall of the tank. Peric and Zorn [7] studied structural impact of sloshing loads caused by arbitrary motion of tank. The numerical simulation shows agreement with the experiment. It is also found that there is negligible difference between in result in turbulence and laminar model. Tyagrajan et al. [9] worked on a sloshing in a rectangular tank using sway excitation. It was observed that 20% and 80% causes higher pressure than other condition. Hou et al. [10] applied multiple excitation on a rectangular tank and concluded that liquid sloshing become violent and intensified if sloshing tank is under multiple coupled excitations. Wang and Khoo [11] worked on sloshing in a 2d rectangular tank using fully nonlinear wave velocity potential theory based on the finite element method.

Minimizing slosh noise in automobile industry is one of the broad area of research Stefan aus der Wiesche [12] establish co-relation between slosh noise intensity and the pressure fluctuations.

Wachowski et al [13] demonstrate various type of noise in automotive fuel tank and concluded that optimisation of the tank structure can achieve lower noise emissions and vibration.

1.3 Objective

1.The main objective is to develop a methodology to numerically predict slosh noise. I am doing the CFD study and validate CFD result with experimental data. My others colleagues will predict noise from acoustic software.

2. In the first part of thesis numerical simulation result validated with Hintasu et al [8] work and then various parametric study such as grid independence study, time independence, viscous effect, 2D vs 3D, effect of fluid fill level, time period and amplitude have been done.

3.In the second part of thesis numerical result validated with our experimental set up .

1.4 Outline

Chapter 1 describes sloshing and sloshing noise. The basic acoustic model of fuel tank has been carried out.

Chapter 2 deals with the governing equations in sloshing case. In this chapter turbulence modeling fluid property has been described.

Chapter 3 deals with computational grid and procedure for solving the sloshing case in STARCCM+ software. There is also brief description given of experimental set up.

Chapters 4 deals with result and discussion. It consist validation of CFD result with Hinatsu et al [8] work. Then grid independence study, time independence study, viscous effect have been done. In this chapter various parametric study for example effect of filling level, effect of amplitude, effect of amplitude have been discussed. Finally our experimental set up result validated with STARCCM+ software.

Chapter 2

Mathematical Model

2.1 Governing equations

The Volume of fluid method developed by Hirt and Nichols [14] is used to capture free surface. The VOF method is based on a fact variable and property in given cell are either represent on one phase or mixture of phases depending upon volume fraction. Volume of fraction is defined as ration of volume of phase in cell to volume of cell. The VOF is based on a characteristic function α which represents volume of fraction of a cell filled liquid. Thus there are 3 possibilities

$$\alpha = 0 \text{ (Cell is empty)}$$

$$\alpha = 1 \text{ (Cell is filled)}$$

$$0 < \alpha < 1 \text{ (Cell is partially filled with liquid and air)}$$

The volume of fluid equation

$$\frac{\partial \alpha}{\partial t} + u_i \frac{\partial \alpha}{\partial x_i} = 0 \quad (2.1)$$

with

$$\rho_1 + \rho_2(1 - \alpha) = 1 \quad (2.2)$$

$$\mu_1 + \mu_2(1 - \alpha) = 1 \quad (2.3)$$

where ρ is density and μ is viscosity.

The fluid is assumed incompressible, surface tension and cavitation neglected. The incompressible Navier -Stokes equations will use to describe the sloshing behavior of a fluid in general term. They are based on conservation of mass and momentum-

$$\frac{\partial u_i}{\partial x_i} = 0 \quad (2.4)$$

$$\frac{\partial u_i}{\partial t} + u_j \frac{\partial u_i}{\partial x_j} = -\frac{1}{\rho} \frac{\partial p}{\partial x_i} + \nu \frac{\partial^2 u_i}{\partial x_j \partial x_j} + b_i \quad (2.5)$$

Where b_i is the body force, ν kinematic viscosity, ρ is fluid density, p pressure, t time and u_i the velocity vector.

The advection scheme is important to get sharp interference. When we choose the advection scheme the order of scheme is important. Lower order scheme will cause numerical diffusion while higher order scheme will give numerical oscillation. To avoid both situation HRIC (High Resolution Interference Scheme) will be used to get sharp interference. It is based on NVD (Normalized Variable Diagram).The NVD is very useful to analyzing boundless propertied of convective discretization scheme. Figure 2.1 shows NVD diagram. The nodal value is labeled $\alpha_D, \alpha_C, \alpha_U$ which represent downward, central, upward. α_f denotes the face of the control volume.

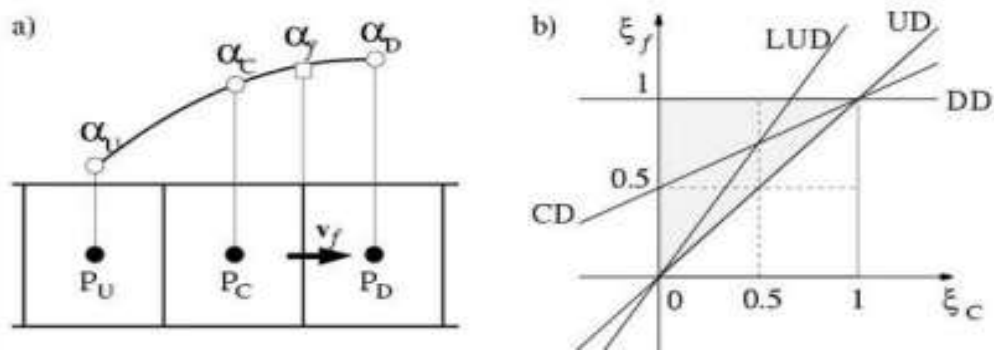


Figure 2.1

The normalized face variable in the vicinity face f is defined as

$$\varepsilon(r,t) = \frac{\alpha(r,t) - \alpha_U}{\alpha_D - \alpha_U} \quad (2.6)$$

The normalized face value

$$\varepsilon_f = \frac{\alpha_f - \alpha_U}{\alpha_D - \alpha_U} \quad (2.7)$$

$$\varepsilon_c = \frac{\alpha_c - \alpha_U}{\alpha_D - \alpha_U} \quad (2.8)$$

HRIC scheme is based on NVD diagram. HRIC scheme consist three steps. In the First step ,the normalized cell face value will be found. The normalize face value is given by.

$$\varepsilon_f = \left\{ \begin{array}{ll} \varepsilon_c & \text{if } \varepsilon_c < 0 \\ 2\varepsilon_c & \text{if } 0 < \varepsilon_c < 1 \\ 1 & \text{if } 0.5 < \varepsilon_c < 1 \end{array} \right\} \quad (2.9)$$

$$\varepsilon_f^* = \left\{ \begin{array}{ll} \varepsilon_f & \text{if } Cu < Cu_l \\ \varepsilon_c + (\varepsilon_f - \varepsilon_c) \frac{Cu_u - Cu}{Cu_u - Cu_l} & \text{if } Cu_l \leq Cu < Cu_u \\ \varepsilon_c & \text{if } Cu_u < Cu \end{array} \right\} \quad (2.10)$$

By default Cu_l is chosen 0.5 and Cu_u is choose 1.If $Cu < Cu_l$ then HRIC will be used. If $Cu_l < Cu < Cu_u$ then HRIC and UD will be applicable .If $Cu_u < Cu$ then UD is used. To control diffusion sharpening factor kept 0.2.

2.2 Modeling time

Implicit unsteady model has been used for sloshing phenomena. Implicit method solves the equation using current time step and later time step. The main advantage of implicit model is that it needs fewer time steps are carry out the calculation over given time interval. The disadvantage is that computer time per step is large than the explicit time step.

Pressure based segregated solver use to solve the governing equation. In pressure based segregated solver used to solve the equation sequentially from each other. To solve segregated solver the each iteration consist step which shows below-

(1) First we update fluid properties (eg, density, viscosity, specific heat,) based on the current solution.

(2) Use the updated values of pressure and face mass fluxes. To solve the momentum equations one after another.

(3) Using the pressure correction obtained from Step 3 correct face mass fluxes, pressure, and the velocity field

(4) Solve the equations for additional scalars turbulent energy and dissipation rate using the current values of the solution variables.

(5) Now update the source terms.

(6) Now check for the convergence of the equations.

These steps are continued until the convergence criteria are met.

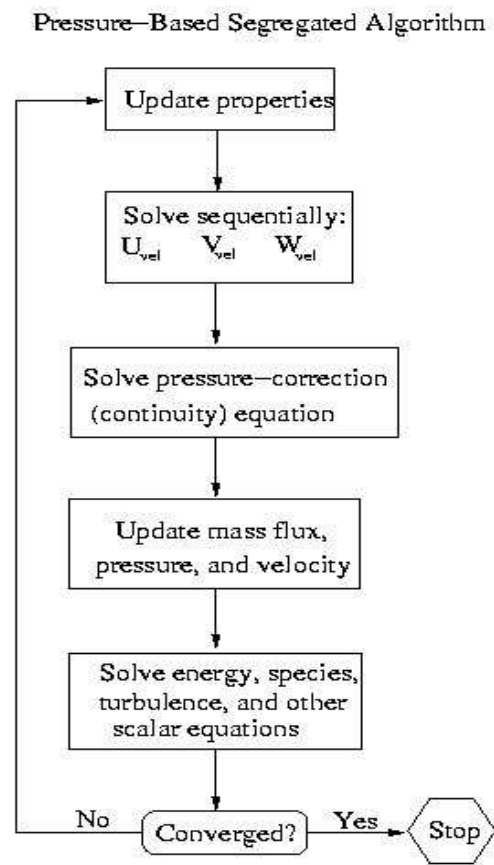


Figure : 2.2

In the present case a 3D rectangular tank of dimension $1200 \times 600 \times 200\text{mm}$ has been considered. The tank is filled with 20% liquid. There is 3 pressure probes have been fitted at different location of tank. The computational results are compared to Hinatsu et al [8] experimental data to carry out a series of sloshing experiments at the National Maritime Research Institute of Japan. Figure 2.3 shows 3D rectangular tank.

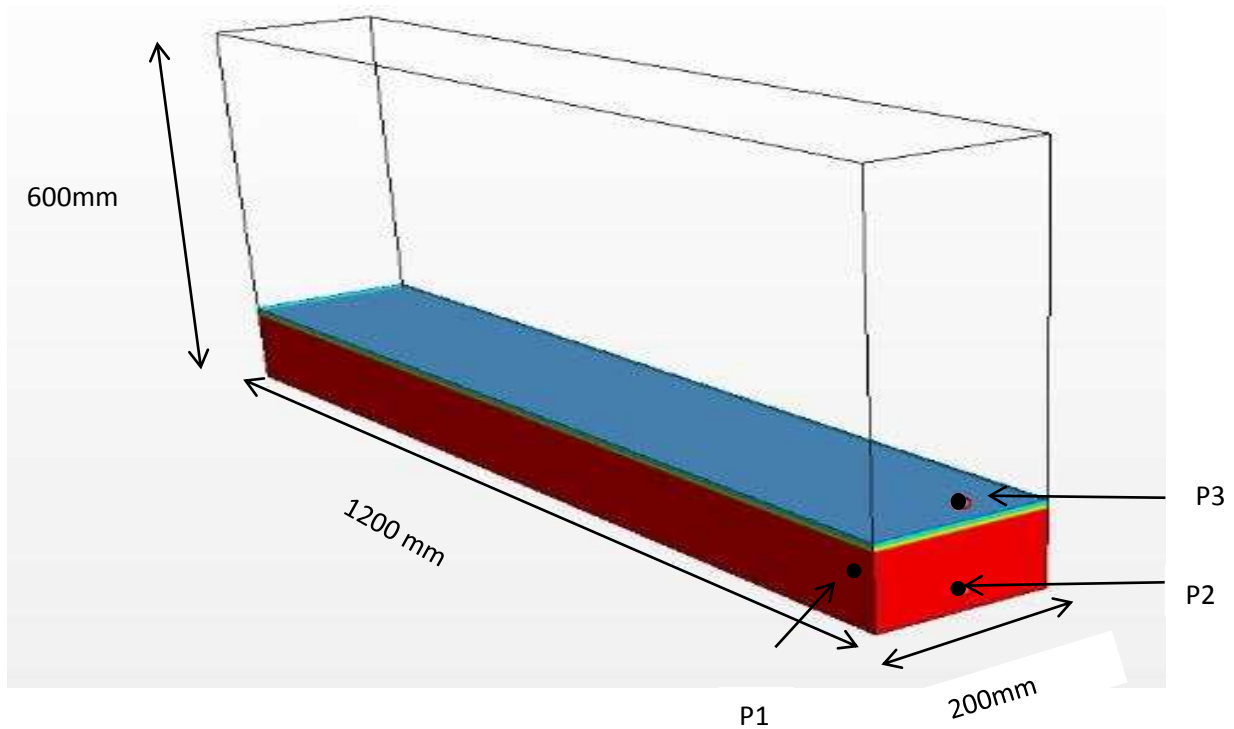


Figure 2.3 : 3D rectangular tank

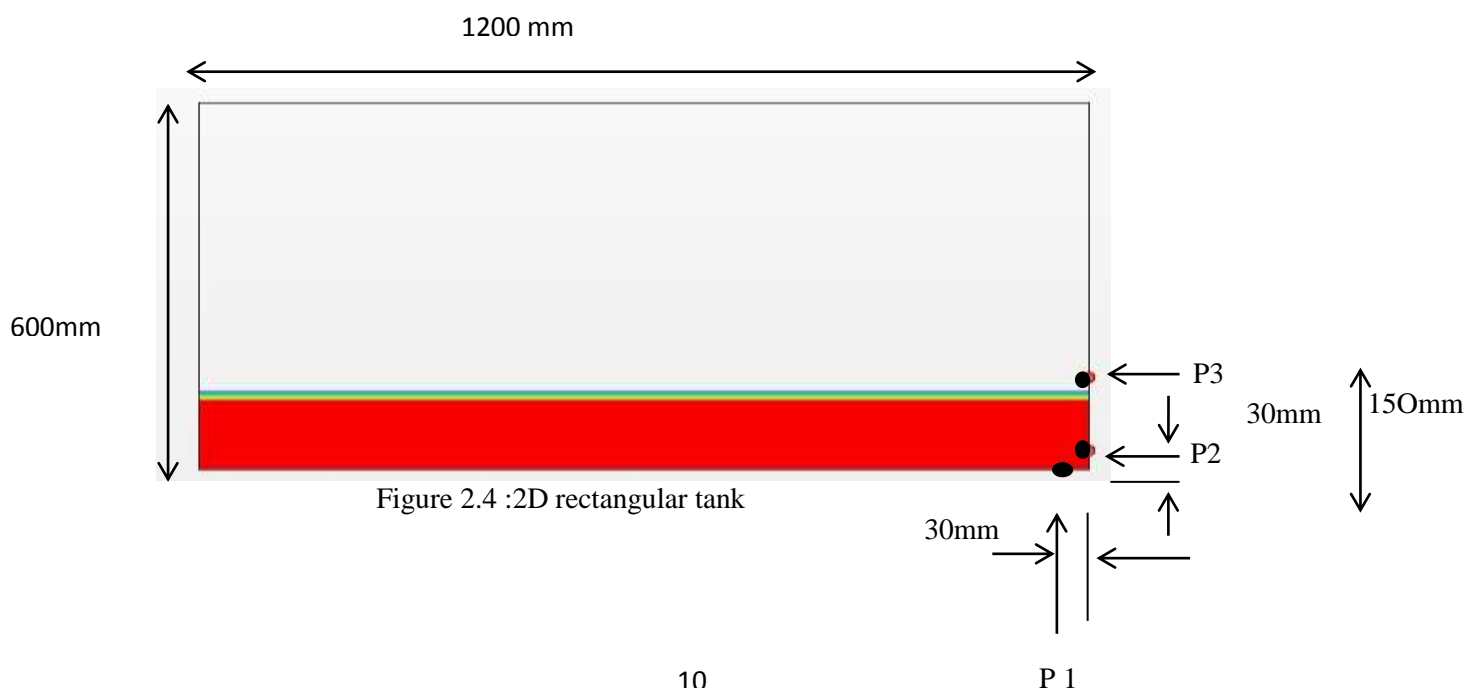


Figure 2.4 :2D rectangular tank

Body force approach is used to applied force in x direction only. The tank displacement is given by

$$x = A\omega\sin(\omega t) \quad (2.11)$$

Where $A = 60$ mm is displacement amplitude, $T = 1.74$ second is time period, ω is the angular frequency and t is elapse time.

So that acceleration of tank is given by

$$F = -A\omega^2\sin(\omega t) \quad (2.12)$$

Using equation (2.5) Navier Stokes equation is given by

$$\frac{\partial u_i}{\partial t} + u_j \frac{\partial u_i}{\partial x_j} = -\frac{1}{\rho} \frac{\partial p}{\partial x_i} + \nu \frac{\partial^2 u_i}{\partial x_j \partial x_j} + b_i \quad (2.13)$$

Where b_i is body force it contains the body approach for eg gravity $(F, -9.81, 0.0)$. For present case the Navier Stokes equation is given by

$$\frac{\partial u_i}{\partial t} + u_j \frac{\partial u_i}{\partial x_j} = -\frac{1}{\rho} \frac{\partial p}{\partial x_i} + \nu \frac{\partial^2 u_i}{\partial x_j \partial x_j} + (F, -9.81, 0.0) \quad (2.14)$$

Where F is acceleration in x direction derived in equation (2.6).

The natural frequency of tank is given by

$$\omega_n^2 = (\pi g / a) \tanh(\pi h / a) \quad (2.15)$$

Where ω_n is natural frequency, a is length of tank, h is fluid level height. When external excitation is equal to natural frequency this called resonance condition. In this condition the sloshing behavior of liquid violent sloshing fluid becomes more irregular

2.3 Fluid property

Fluid property plays important role during the sloshing phenomena. For most of cases water and air uses with clearly defined property. Viscosity plays important roll for small excitation and high filling level[2]. The Reynolds number is given by

$$Re No = \frac{\rho UL}{\mu} \quad (2.16)$$

Where ρ is density, μ is dynamic viscosity, L is characteristic length. The typical value of dynamic viscosity of water is $8.8887E-05$ pa-s and density is $997.561 \text{ kg}/m^3$. The typical value of dynamic viscosity of air is $1.85E-05$ pa-s and density is $1.18415 \text{ kg}/m^3$.

2.4 Boundary condition

In CFD boundary condition is necessary to solve the differential equation and Neumann boundary condition is generally used in CFD to solve the equation. In Dirichlet boundary condition the solution needs to take at boundary of domain. In fluid mechanics point of view it is same as no slip boundary condition. In present case no slip boundary condition applied. It is assume that fluid velocity is same velocity of wall. In Neumann boundary condition derivative of solution takes place on boundary of domain. As the computational domain fully enclosed a reference pressure is defined at center of top wall of tank.

2.5 Turbulence Modeling

Turbulence is characterized by pressure; velocity and other quantity fluctuate with respect to time and space. When turbulence is present in any flow it dominant all other phenomena and it increase dissipation of energy and heat transfer and drag. The Reynolds number is given by

$$Re\ No = \frac{\rho UL}{\mu} \quad (2.17)$$

Where U is characteristic velocity = 0.2 m/s, L is characteristic length = 1.2 m, μ is viscosity = 8.8887E-05 pa-s, ρ is density is 997.561 . For above case it is clear that it is turbulence. But there is not significant variation in result whether sloshing model should be laminar or turbulence. There is some author like Price and Chen [15] assumed flow to be laminar while El Moctar [16], Rhee [17] and Standing et al. [18] assumed the flow to be turbulent. In present case for sloshing turbulence model is used.

Turbulence is generally characterized by large time and length scale. So to reduce its complexity it time averaging the turbulence effects are incorporated in terms of the mean quantities of the flow.

Instantaneous velocity
$$u_i = U_i + u_i'$$

Where U_i is the mean velocity and u_i' fluctuating component

By substituting these values in Navier Stokes equation the Reynolds-Averaged Navier Stokes Equation (RANS) is obtained.

$$\frac{\partial u_i}{\partial x_i} = 0 \quad (2.18)$$

$$\rho \frac{\partial u_i}{\partial t} + \rho u_j \frac{\partial u_i}{\partial x_j} = \frac{\partial p}{\partial x_i} + \frac{\partial}{\partial x_j} u_i \left[\frac{\partial u_i}{\partial x_j} + \frac{\partial u_j}{\partial x_i} + \tau_{ij} \right] + b_i \quad (2.19)$$

where ρ and μ are the density and dynamic viscosity of the fluid b_i is the net body force acting over the domain and u_i are the components of free stream velocity acting in x and y directions

respectively. τ_{ij} is the Reynolds stress which is found by Bossinius hypothesis. According to Bossinius hypothesis the Reynolds stress tensor is proportional to mean rate tensor.

$$\tau_{ij} = \mu_t \left(\frac{\partial u_i}{\partial x_j} + \frac{\partial u_j}{\partial x_i} \right) - \frac{2}{3} k \delta_{ij} \quad (2.20)$$

Where μ_t is turbulence viscosity

$$\mu_t = \rho C_\mu \frac{k^2}{\varepsilon} \quad (2.21)$$

Where $C_\mu = 0.09$, k = Turbulence kinetic energy and ε = Turbulence dissipation rate, δ_{ij} = chronicle delta.

Turbulence k – ε model is one of the most widely used turbulence models in CFD. It requires two additional transport equations, a notable increase in required computational effort. Reynolds stress is found by using turbulence kinetic energy k and using dissipation rate ε . Transport equation of turbulence k – ε model is given by

$$\rho \frac{\partial k}{\partial t} + \rho u_j \frac{\partial k}{\partial x_j} = \tau_{ij} \frac{\partial u_i}{\partial x_j} - \rho \varepsilon + \frac{\partial}{\partial x_j} \left[\left(\mu + \frac{\mu_t}{\sigma_k} \right) \frac{\partial k}{\partial x_j} \right] \quad (2.22)$$

$$\rho \frac{\partial \varepsilon}{\partial t} + \rho u_j \frac{\partial \varepsilon}{\partial x_j} = C_{\varepsilon 1} \frac{\varepsilon}{k} \tau_{ij} \frac{\partial u_i}{\partial x_j} - C_{\varepsilon 2} \rho \frac{\varepsilon^2}{k} + \frac{\partial}{\partial x_j} \left[\left(\mu + \frac{\mu_t}{\sigma_\varepsilon} \right) \frac{\partial \varepsilon}{\partial x_j} \right] \quad (2.23)$$

Where $C_{\varepsilon 1} = 1.44$, $C_{\varepsilon 2} = 1.92$, and $\sigma_k = 1.00$, $\sigma_\varepsilon = 1.30$ constant value.

It is used in industrial type of application which contains complex recirculation with or without heat transfer. It is also useful for free shear layer flow. There are also many weakness of k ε model-

- (1) It is limited to small pressure gradient. It does not work In large pressure gradient.
- (2) It faces difficulty to model complex shear.

Turbulence intensity is and important parameter for set boundary condition in CFD simulation. It is defined as ration of RMS value of turbulence velocity to mean velocity. Turbulence intensity value lied between 0.01 to 0.1. To estimate turbulence insanity there is three parameter

(1) High-turbulence case: For the high turbulence case and complex geometry turbulence insanity value varied between 5% and 20%.

(2) Medium-turbulence case: For low Reynolds number flow and not complex geometry turbulence intensity value between 1% and 5%.

(3) Low turbulence case: For submarines and aircrafts turbulence intensity value below 1%. For present problem because it is not so complex geometry turbulence intensity kept 1%.

Turbulence viscosity ratio is defined as ration of turbulence viscosity ratio to dynamic viscosity. Turbulence viscosity is an important parameter for low turbulence case where it is difficult to guess turbulence length. Turbulence viscosity ratio is given b

$$\beta = \frac{\mu_t}{\mu} \quad (2.24)$$

For my case turbulence viscosity chosen 10.

2.6 Wall function

To resolve boundary layer near the wall function has been used. For it y^+ value is an important parameter for meshing requirement. As figure shows that y^+ value should be chosen such that it should be not so much high so it cross the boundary layer and also its value should be not so much small so it comes inside viscous sub layer. So it should be chosen carefully otherwise it will create problem at first node and it will cause error at pressure drop and velocity.

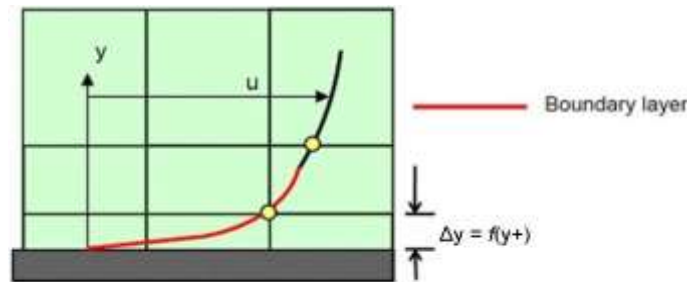


Figure 2.5

High Reynolds numbers flows for instance aircraft experience a logarithmic boundary layer that extends to several thousand y^+ units. Low Reynolds number flows eg as turbine blades may contain 100 y^+ units. In practice, this means that the use of wall functions for these class of flows should be avoided as their use will limit the overall number of mesh nodes that can be sensibly placed within the boundary layer. So the main question is that how to choose value. The y^+ value is given by

$$y^+ = \frac{\rho \Delta y u_t}{\mu} \quad (2.25)$$

Where ρ is density, Δy is distance from wall, u_t friction velocity and μ is viscosity.

$$u_t = \left(\frac{\tau_w}{\rho} \right)^{0.5} \quad (2.26)$$

Where τ_w is the shear stress. For high Reynolds number the y^+ first near-wall grid point is varies between $20 < y^+ < 100$ while for low Reynolds number its value $y^+ < 1$.

Chapter 3

Computation grid and solution procedure

3.1 Computational Grid

A mesh or grid is defined as a set of point which distributed over the problem domain. The grid or mesh plays important roll to predict accuracy of solution CFD. In CFD 50 % time is for only generation of grid. For eg when problem geometry is irregular, mesh which closely fit the boundary enable a better implantation of boundary than a rectangular meshes which envelope the domain. In letter case cell near to boundary will be incomplete. In such type of cases a tedious interpolation is needed to full fill boundary conditions. So that solution obtained by body fitted grid is more accurate that rectangular mesh envelopes on irregular geometry.

Grid generation is static process means that grid should be generated before starting numerical solution procedure. Static grid generation used requirement is to produce body fitted grid for complex geometry. When it is requirement to tracked moving fronts accurately adaptive grid generation has been used. The demand placed to grid point distribution vary from problem to problem. For body fitted grid it is necessary that grid lines fits the boundary of the geometry and smoothly interior region of .It is also necessary to make intersecting grid lines orthogonal to each other. The numerical solution will be highly inaccurate if the angle between grid line is close to zero. While in the adaptive grid primary interest is on grid spacing

3.1.1 Classification of Grids

3.1.1.1 Structured type

For structure type of grid following point is notable

- (a) In structure gird every grid point represent as a origin because gird points are located at intersection of grid lines.
- (b) They have fixed number of neighboring point.
- (c) In structured grid neighbors are can be easily identified so that speeds up the solution.

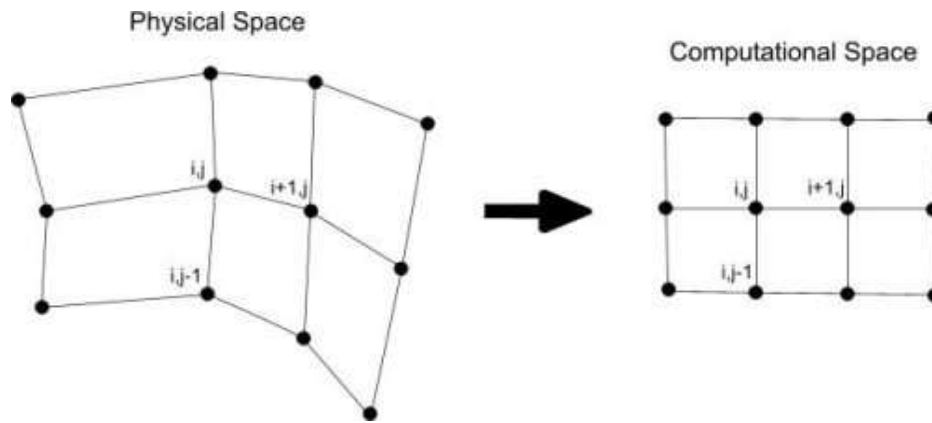


Figure 3.1:Structural grid

In structural grid because neighbors are fixed complex physical domain is changed into simple computational. Structural grid consist non -orthogonal and curvilinear coordinates so that each segment is described by a constant value of one of the curvilinear and entire mesh is formed by intersection of curvilinear coordinates lines. Structural grid is generally uses for finite difference or finite volume method. Because grid lines are orthogonal in transformed geometry so all governing partial difference equation is transferred into their equaling form.

In structural grid mapping function is possible means the way computer store the data. Figure 3.1 shows a structural grid there mesh is aligned in a specified pattern. In Figure 3.1 if point is added in midway between (i,j) and $(i+1,j)$, Point must be added between $(i,j+1)$ and $(i+1,j+1)$, and also between $(i,j-1)$ and $(i+1,j-1)$. Otherwise, middle row of points would have one more than the others, and the mesh structure would be broken.

Three basic grid configuration for structural meshing-

(a) O –type grid

In O- type grid looks like O word. In this type of grid last point of grid wraps around and meets with the first point. Figures shows 3.2 O –type grid

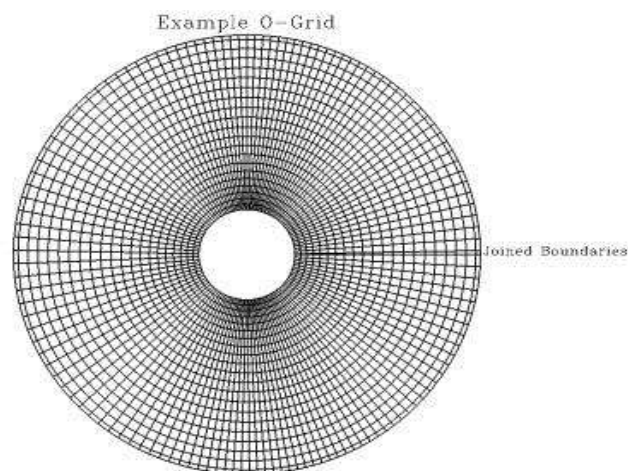


Figure 3.2:O grid

(b) C- type of grid

C-grid are shaped like the letter “C”, and they have line which typically meets with at bend back to meet up with itself at some point. In the example below, the line which describes the airfoil surface meets at the trailing edge.

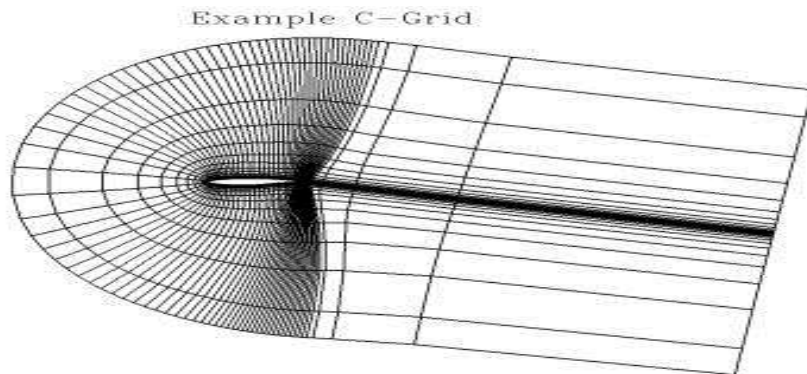


Figure 3.3:C grid

3.1.1.2 Unstructured grid

In unstructured grid there is no mapping is possible. In unstructured grid there is no physical relation between n and $n+1$ node. It means that there no physical relationship maintained between typical node and its neighbors. It means that in unstructured grid need more time to solve the problem.so that unstructured grid is mainly used in FEA analysis.

Unstructured grid is very easy to generate. So most of commercial software uses the unstructured grid to solve the problem. It is possible to convert structured grid into unstructured grid but its vice versa is not possible.

Use of unstructured grid allows us to avoid any quadrilaterals (in 2-D—hexahedrons in 3-D) the way you do in structured grids. Few unstructured CFD solvers like USM3D uses only tetrahedral grid .But most of other software provide facility to build grids with different cell shape. Few examples show below.

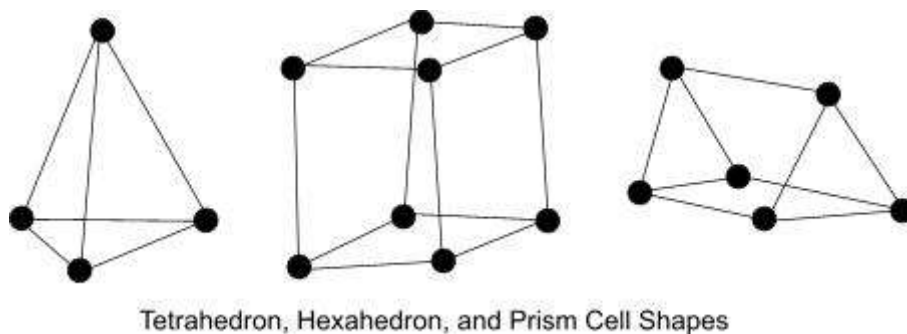


Figure 3.4: Unstructured grid

Unstructured Cartesian mesh is another example of unstructured grid. To construct Unstructured Cartesian mesh it start with building few square cell which is subdivided into smaller cubes. The figure shows mesh around half cylinder-

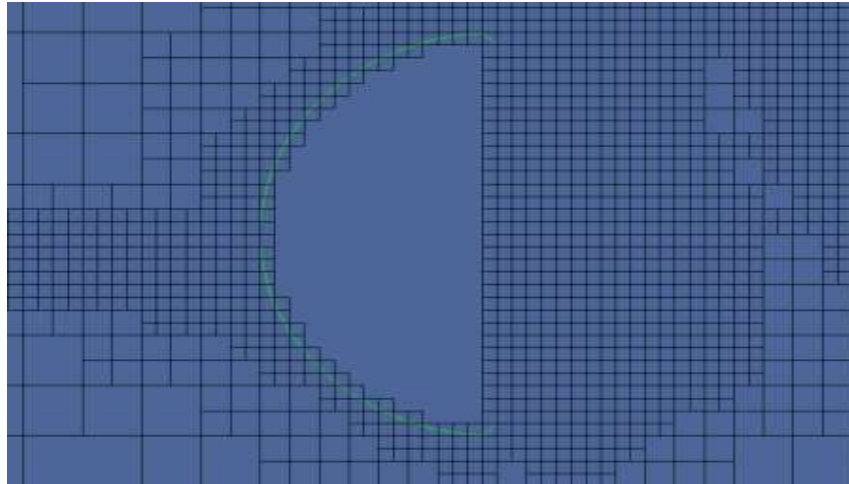


Figure 3.5: Unstructured Cartesian mesh

One of the most striking features of unstructured Cartesian meshes is that cells around the body do not exactly follow the body. The solvers which employ this grid technique use “immersed boundaries” to handle curved surfaces.

There is another type of grid is Hybrid grid. For most of complex geometry this type of grid uses. In this type of grid the top most portion of grid is square and triangle because shape is very complex so want capture the whole shape by single element so that multiple grid is needed. The hybrid grid is given below

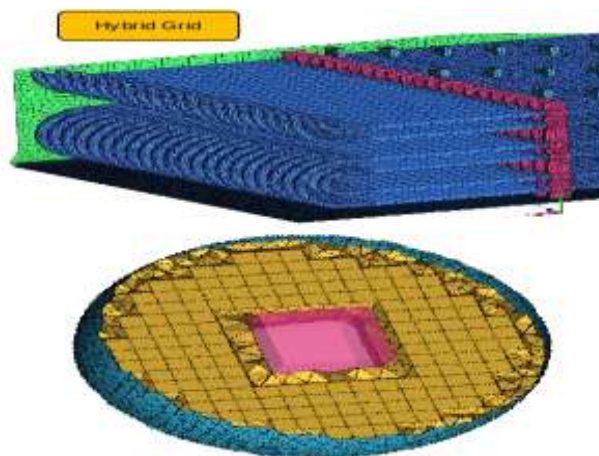


Figure 3.6: Hybrid grid

3.2 Test Problem computational grid

Computational grid used is shown in Figure 3.2. It consists of 8192 cells, 16192 interior faces and 8385 vertices. For with Hinatsu et al [8] work 128×64 grid has been used. Grid independence has been discussed in next chapter.

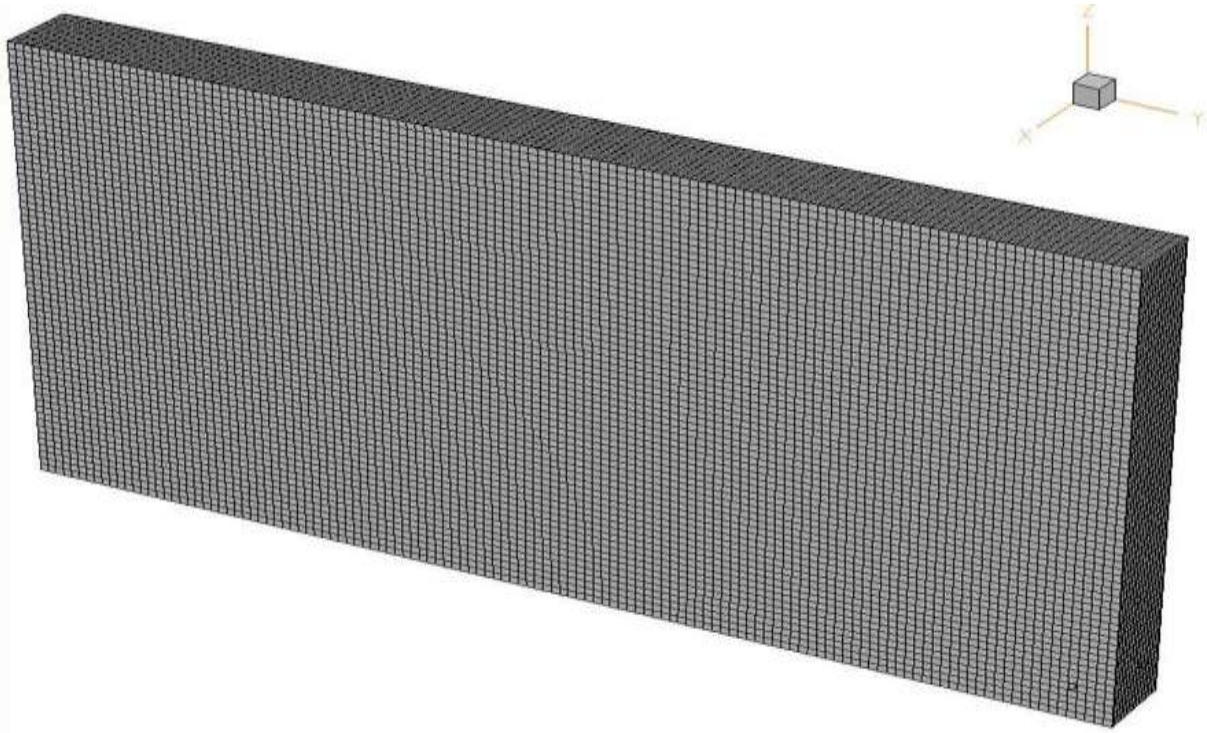


Figure 3.7: Test problem grid

To generate this mesh there is surface remesher, trimmer and prism layer has been used. The description of it is discussed below

(1) Surface remesher

If the requirement of problem is to improve the overall quality of the surface and to re-triangulate an existing surface surface remesher is used. Surface remeshing is mainly based on a target edge length. It contains various refinement feature based on curvature and surface proximity. The surface remesher is typically used for remeshing when the surfaces is produced by the surface wrapper and STL data. Surface remesher mainly used when high level of accuracy needed in problem and when it contains very bad quality of triangle.

There is various meshing control tool is available in surface remesher which can control during the meshing process.

(a) Global value-

- (i) Base size- The base is length of a one cell. For present case it is 9.735 mm.
- (ii) Cad Projection –The CAD projection node is turned off. It does allow vertices to be projected back to the imported CAD surface during surface remeshing.
- (iii) Automatic surface repair- This option automatically correct the geometry if there is any problem in any geometry.
- (iv) Surface curvature- This node provide facility for refinement of cell for surface remesh models which is based on number of points around the circle and the curvature deviation distance. It is turned off
- (v) Surface growth rate- This parameter controls the rate of triangle edges size from one cell to its neighboring cell. For present case it kept 1.3.If its value increase then it will produce less triangle and if its value decrease it will generate more triangles
- (vi) Surface proximity- It allows the refinement of cell based on search distance and number of points in a gap. Points in gap value is used for specifying the refinement for surface that are close to one another.

(b) Boundary level

This node allows to specify different parameter to control the surface remesh at different boundary surface. These parameter are

- i) Custom surface curvature- It allows the surface curvature setting at the boundary.
- ii) Custom surface proximity- It allows the surface proximity at boundary.
- iii) Custom surface size- It allows to set surface minimum, maximum and target edge sizes at the boundary.

(2) Trimmer

Trimmer mesh used to produce high quality of grid for simple and complicated geometry both. Trimmer mesh contain hexahedral cells which trims the core mesh. It can be refined by using curvature and proximity.. Its growth parameter can also be control. A maximum and/or minimum cell size can be supplied as well to control the upper and lower cell size bounds.

The choice of meshing model depend on to get minimum skewness and reduce the numerical error. There is two type of trimmer template mesh is available-

- (i) Hexahedral – In this type of template hexahedral shape cells will be used. For present case hexahedral cell has been used.
- (ii) Dodecahedra- In this type of cell it will consist 12 faces and each faces composed of 4 equal length.

Growth rates allow controlling the rate of changing of cell size from one cell to another cell. A slow growth rate means cell sizes will be changed slowly while in fast growth rate cell sizes will be changed rapidly. There are two methods available for growth rate-

- (i) Simple growth rate
- (ii) Two level growth rate

For present case simple growth rate is used.

There is a run optimizer option also available. It should be used when there is poor quality mesh present in the trimmer mesh. It increases the CPU time.

(3) Prism layer- Prism layer is used to enhance the accuracy of result and to align the flow with the mesh. Prism layer allows resolving the turbulent boundary layers. It allows to use high aspect ratio cells thus it provides better cross stream resolution.

Controlling parameters for prism layer

- (i) Thickness of prism layer- It controls the overall thickness of the prism layer. It can be chosen as relative size or absolute size. For present case its absolute value is kept 0.9375 mm.

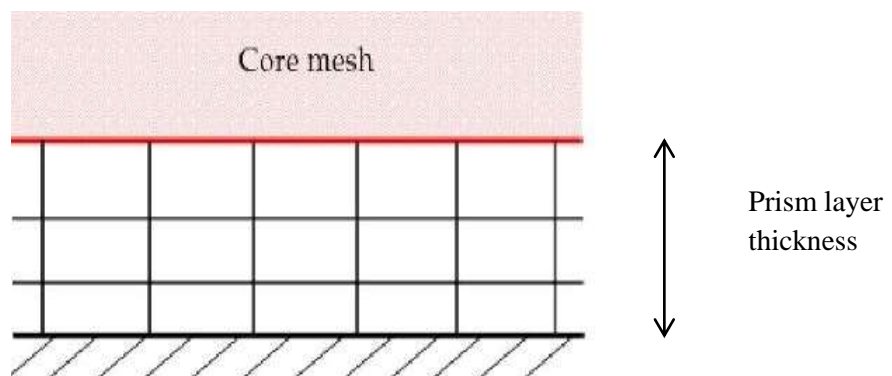


Figure 3.8: Prism layer thickness

- ii) Number of prism layer- It controls the number of prism layers generated on the prism layer. For present case it is kept 2.

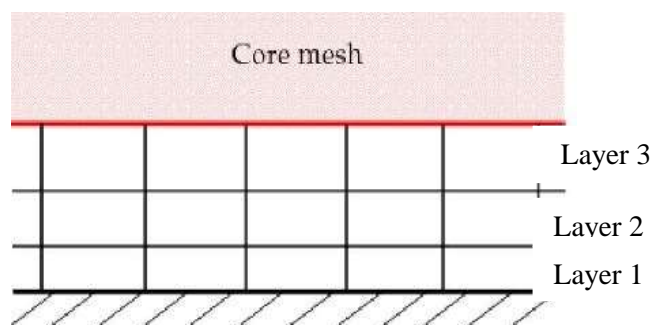


Figure 3.9: Number of prism layer

(iii) Stretching function –It used to generate cell layer thickness .It is the ratio of one cell layer to the thickness of the cell layer beneath. Its minimum value is 1.0. There is two option geometric progression and hyperbolic tangent. Stretch factor is given by = $N2/N1$

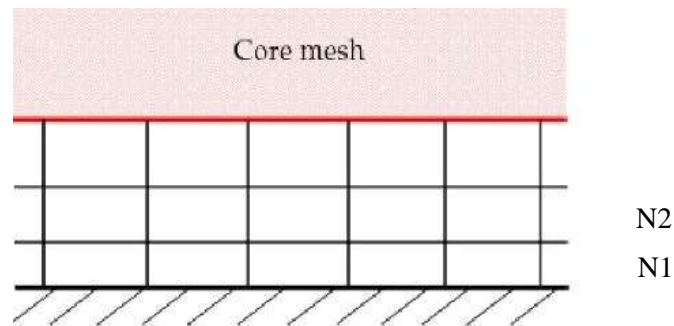


Figure 3.10: Stretching function

(a) Geometric progression- In this option the stretching function is finding by using geometric progression. For present case geometric progression its value kept 1.5.

(b) Hyperbolic tangent- In this option the cell layer found by hyperbolic function which is given by

$$S(n_i) = 1 + \frac{\tanh(F_s \frac{n_i}{N-1})}{\tanh(F_s)} \quad (3.1)$$

Where N = is the total number of layers,

n_i = Current node

F_s = Overall stretching factor

$S(n_i)$ = Distribution value for node

Note that $0 < n_i < N$. For 5 layers n_i takes the values 0, 1,2,3,4,5. The relation between nodes and layers is given below.

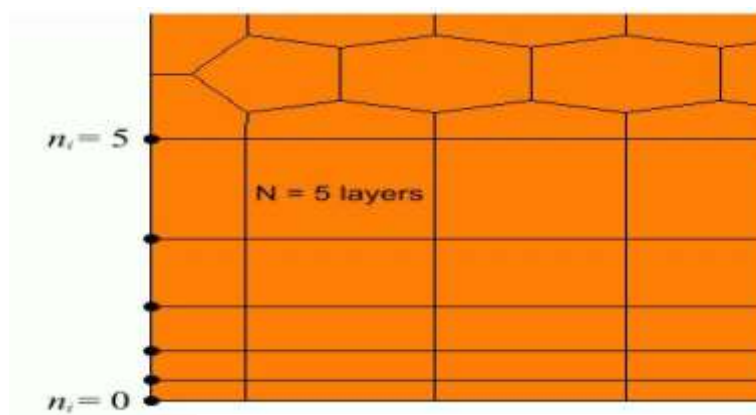


Figure 3.11: Hyperbolic tangent

Geometric progression	≥ 1.0
Hyperbolic tangent	> 0.0

3.3 Numerical solution procedure

STARCCM+ (ver 6.06.011) is a finite volume based CFD algorithm used solve the sloshing problem. STARCCM+ provides best solution for flow problems. STARCCM+ used finite volume method to solve the problem. In finite volume method the domain has divided in control volume and It uses integral form of governing equation. So that it can handle complex problem also. The main difference between finite difference method and finite volume method is that for finite difference method structured grid is required while finite volume method is applicable for complex geometry also. "Finite volume" refers to the small volume surrounding each node point on a mesh. In the finite volume method, volume integrals in a partial differential equation that contain a divergence term are converted to surface integrals, using the divergence theorem. These terms are then evaluated as fluxes at the surfaces of each finite volume. In finite volume the flux leaving the control volume is same as that entering the control volume, so that this methods is conservative. The main advantage of using finite volume method the mass momentum energy can be conserved in coarse grid also.. Gauss divergence theorem used to replace divergence in Navier Stokes equation. Gauss divergence theorem is given by-

$$\iiint \nabla P dv = \iint P ds$$

The most important feature of STARCCM+ is mesh and solve a problem together with over one billion cells. The geometry is also created in STARCCM+ which can subsequently converting to geometry parts for integration with the meshing and simulation process. In present problem there is single region is present which contain several boundary like top, bottom ,inlet, outlet, front, bottom. Three pressure probe has created at different location of tank using derived part option in STARCCM+ in order to measure the pressure at different location. For present problem temporal discretization chosen first order while space discretization chosen second order. For pressure velocity coupling algebraic multi grid with SIMPLE discretization chosen. Under relaxation factor for velocity and pressure has set 0.9 and 0.5.Gauss seidal approach has been used in present sloshing case. For validation with Hinatsu et al [8] work 174762 cells used .After using many time step 1e-4 time step used to validate the result with Hinatsu et al [8].

3.4 Experimental set up

We have Impact test system in lab. In Impact test system there is sudden brake is applied to tank and flow visualization is captured by high speed camera. Figure 3.12 Shows impact test system(ITS).The experimental set up consist rectangular box of dimension of (23.8 × 22 × 23.8cm) filled with water and fully sealed and it runs on a track. Rubber wheel used to minimize friction. The trolley was attached by cable where dead weight can be placed. For present case 1.4 weight used and tank is filled with 20% water. This section treats a particular case of fluid-tank system for further flow visualization and image processing of other cases. The working fluid is water and the container is

filled up to the height of 5.95 cm with water as shown in Figure 3. In order to study the dynamics of the air-water interface, a 2D visualization of flow inside the moving tank was accomplished. The fluid and air water interface motion was examined using a high speed camera. High speed camera placed perpendicular to direction of tank.



Figure 3.12: Impact test system



Figure 13: Impact test system

Chapter 4

Result and discussion

This chapter consist various results. In first part of result is validated with Hinatsu et al [8] result. Then various parameter study have been done. In the second part of result out experimental set up work validated with mine STARCCM+ simulation.

4.1 Grid independence

In the Navier Stokes momentum and energy equations most viscous flow problem consist some nonlinear terms so that solved numerically. A grid(or mesh, the terms are often used interchangeably) is used to represent the problem in computational fluid dynamics usually as a set of finite volume elements. Expertise in the generation of high-quality computational grids has developed alongside CFD and a wide range of literature is available

1. Spacing - The grid should be to be sufficiently fine so that it can solve the conservation of mass and momentum in every cell properly. Fine grid will increase the computational time and memory both. The rate of computational time increase depends on the type of solution algorithm used during simulation. The computational requirements of direct matrix inversion methods grow with $O(n^3)$ cells) but iterative algorithms are around $O(n^2)$ cells). In transient problem the time step also be refined to the grid.

2. Resolution - Grid spacing needs to be sufficiently small to resolve the flow in all regions of the computational domain. This is especially important when using a turbulence model, where the position of the first near-wall grid point can have a significant influence on the CFD output quality. When the grid is too coarse, local flow features are smeared and, especially when considering a sloshing flow, pressure spikes are not resolved with sufficient detail.

3. Geometry- The grid must be should be such that it can provide a sufficiently accurate representation of the geometry used. This becomes very important when there are small changes (e.g. ripples) on a surface, or a body has particular details influencing the flow.

In CFD it always necessary that solution should be independent of grid. If grid is changing solution should not be affected by changing grid. For present problem grid independence has been carried out for 2 dimensional rectangular. There is 4 grid 85,128,192,288 has been studied. Figure 4.1 shows result of grid independence.

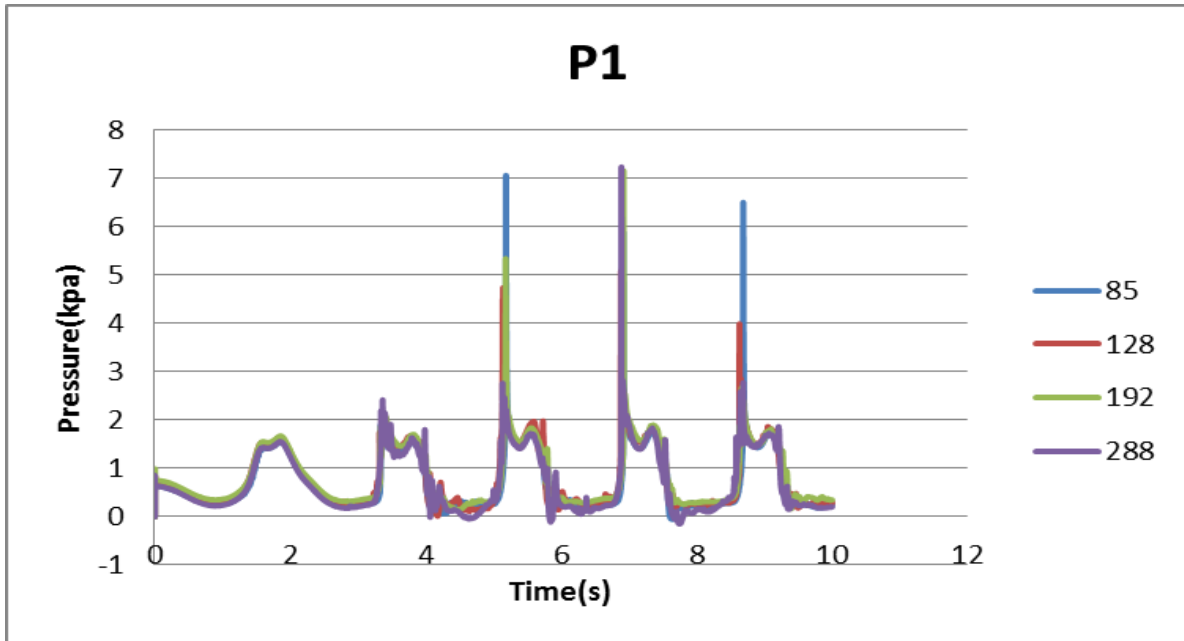


Figure 4.1: P1

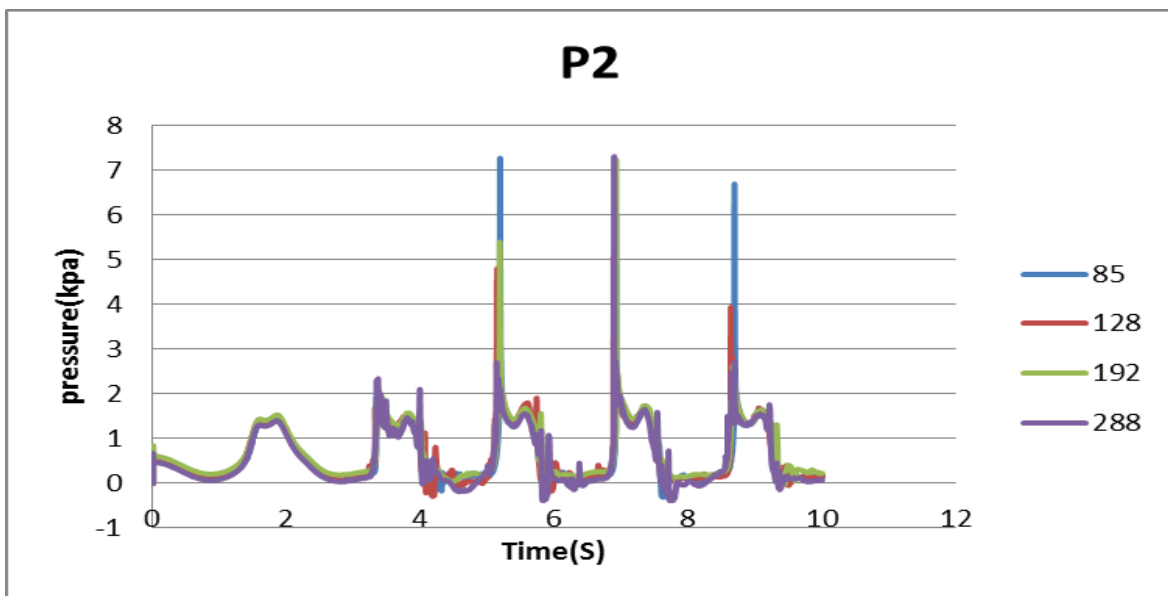


Figure 4.2: P2

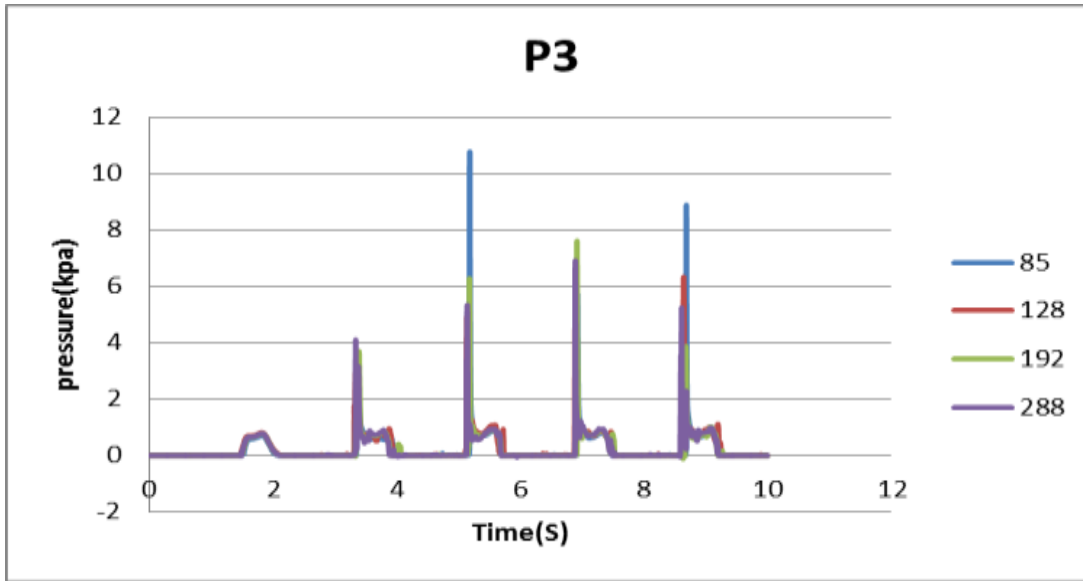


Figure 4.3: P3

Figure 4.1, Figure 4.2 and Figure 4.3 shows the variation of pressure at P1,P2,P3. Figure 4.1 and Figure 4.2 shows that for all four grid initially sloshing is very less so that The first peak is very weak, and the pressure drop after the second peak is gradual. In the third cycle sloshing become prominent so that peaks are higher compare to first cycle. It is happening for all four grid. 85 grid is showing that initially first two cycle maximum peaks are going till 2kpa but letter all cycle the peaks are reaching till 7 kpa. For 128 and 192 grid also same thing is happening. There is slight variation in third cycle the peak is less compare to 85 grid. For 288 grid the time step is also refined to maintain the stability criteria. For Figure 4.3 showing pressure variation for P3. In P3 case for all grid first cycle peaks are very compare to P1,P2 this is because of less amount of water hitting the P3. After first cycle the peaks are higher compare to P1 and P2 because of direct hitting of water with the probe.

4.2 Time Step

The nature of sloshing problem is such that it is always transient. The time derivative in the governing equation should be discretized as well. For present case there is at different time step simulation has run so that optimum time step can be obtained without spending too much computational time and memory. In the sloshing case velocity of the flow of liquid continuously varies throughout the simulation, it is necessary to adjust the time step according to the flow velocity. The Courant number at node is defined as

$$CFL = \frac{C\Delta t}{\Delta x} \quad (4.1)$$

Typically for stable condition $CFL \leq 1$. If the grid size is refining the time step should also be refined according to it to maintain the stability criteria. For present case simulation run for $1E-03$, $1E-04$ and $1E-05$ time step to get optimum time step for simulation.

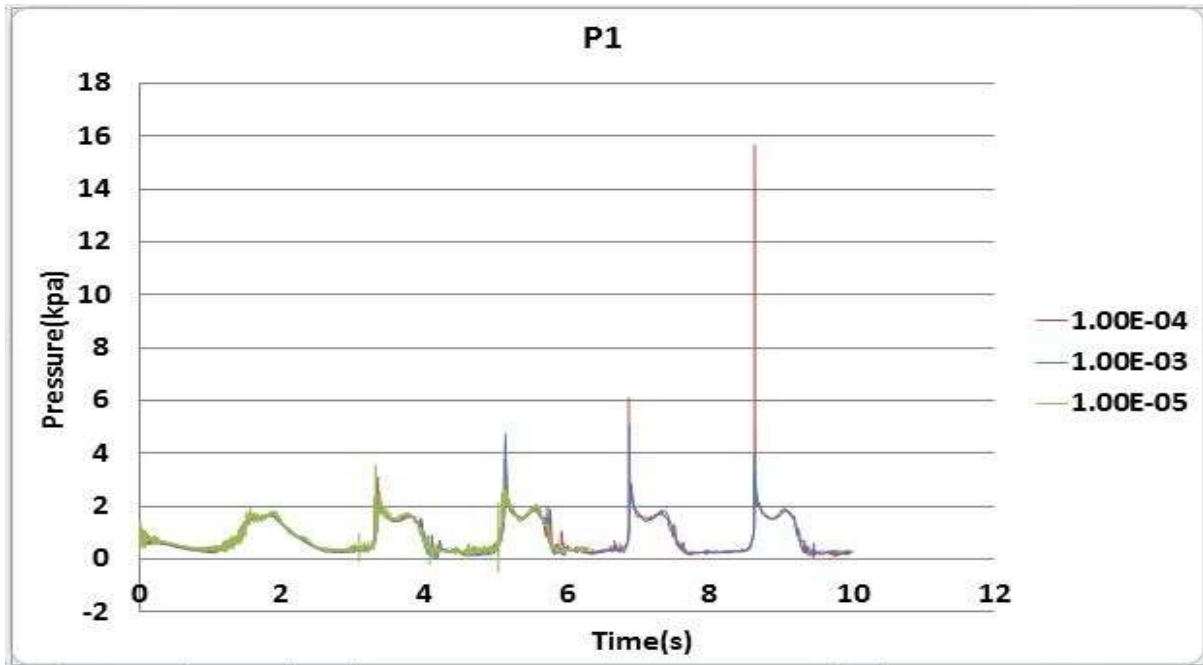


Figure 4.4: P1

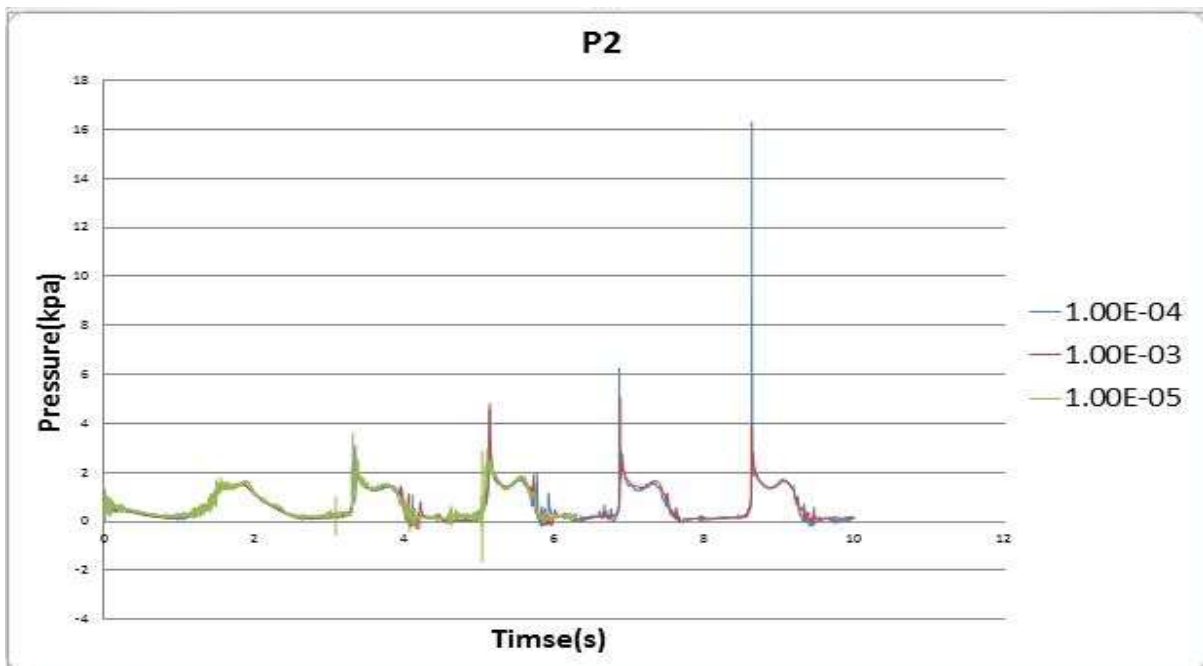


Figure 4.5: P2

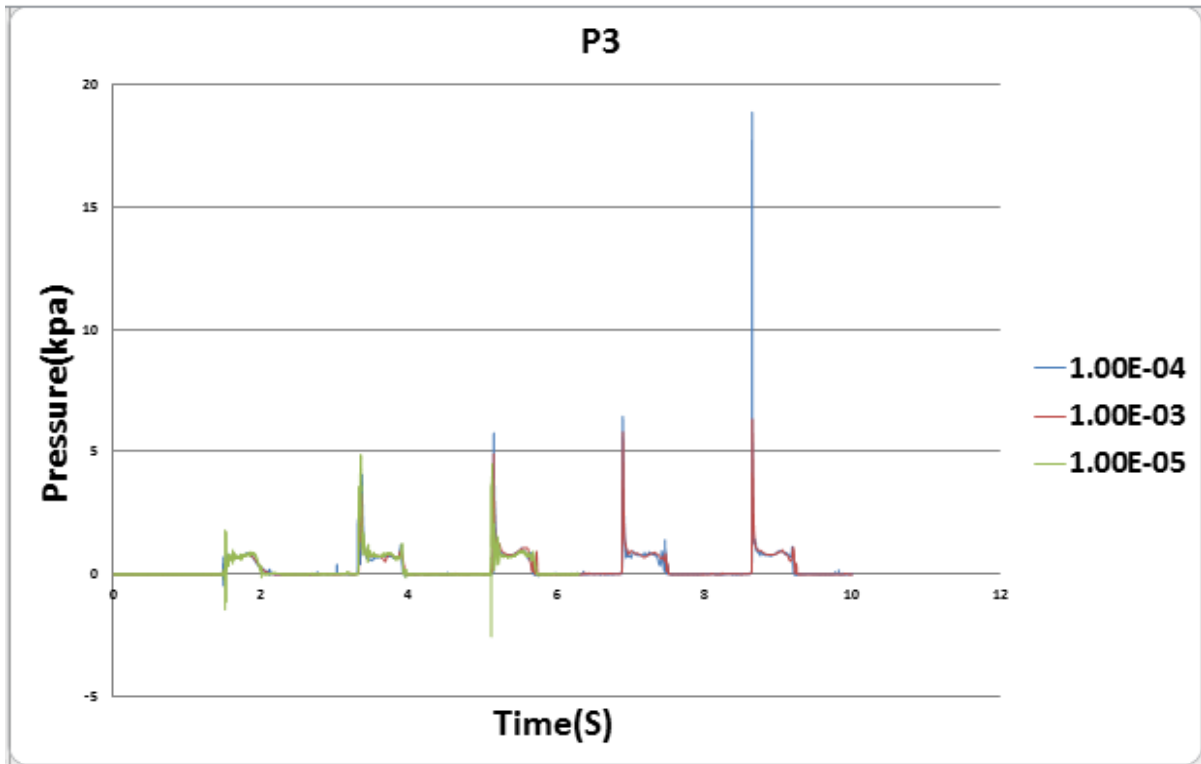


Figure 4.6: P2

Figure 4.4, Figure 4.5, Figure 4.6 shows time independence study for time independence study for 128 grid. Simulation run for using 1E-03 second, 1E-04 and 1E-5 second. Using 1E-05 time step simulation run till 6 second. It observed that using larger time step second pressure peak is less pronounced or even missing. So that using smaller time step like 1E-04 and 1E-05 it is possible to capture small fluctuation also. But choosing smaller time step needed more computational time. So that for validation 1E-04 second chosen.

4.3 Validation

As previously discussed validation work has been done using Hinatsu et al [8] work. For validation on only P2 data is available. The present validation has been using 1E-04 time step, turbulence k-ε model has been. As pattern of pressure variation is not so varying during grid independence so that 128 grid has been chosen. Figure 4.7 shows validation for P2 for 2 dimensional.

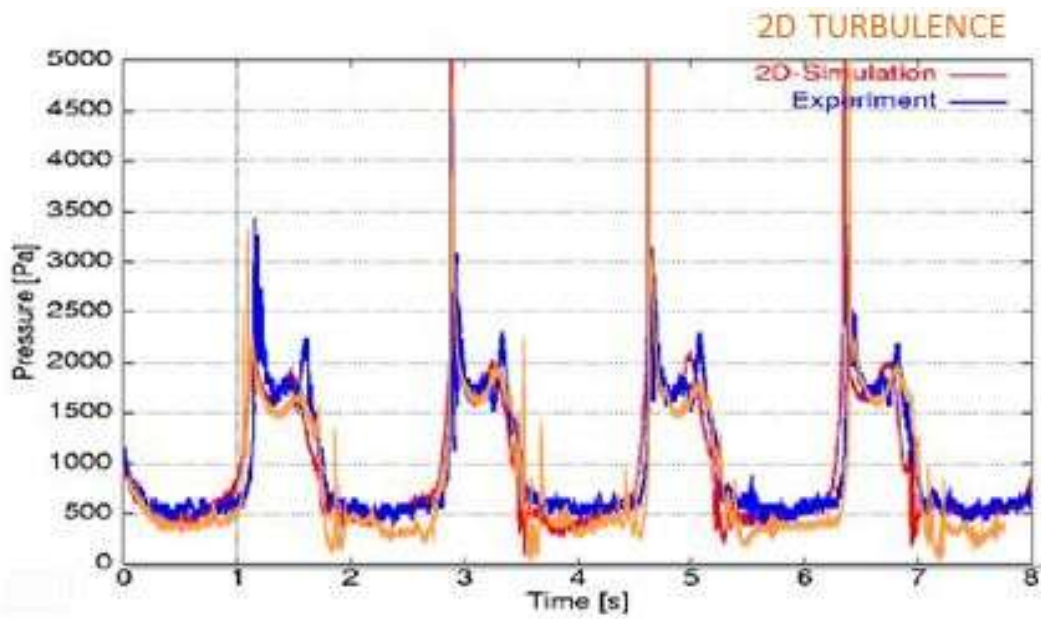


Figure 4.7: Comparison of simulated pressure time series (symbols) to experimental data of Hinatsu et al.[8] for $A=60$ mm, $T=1.74$ second, for P2 for 2D case

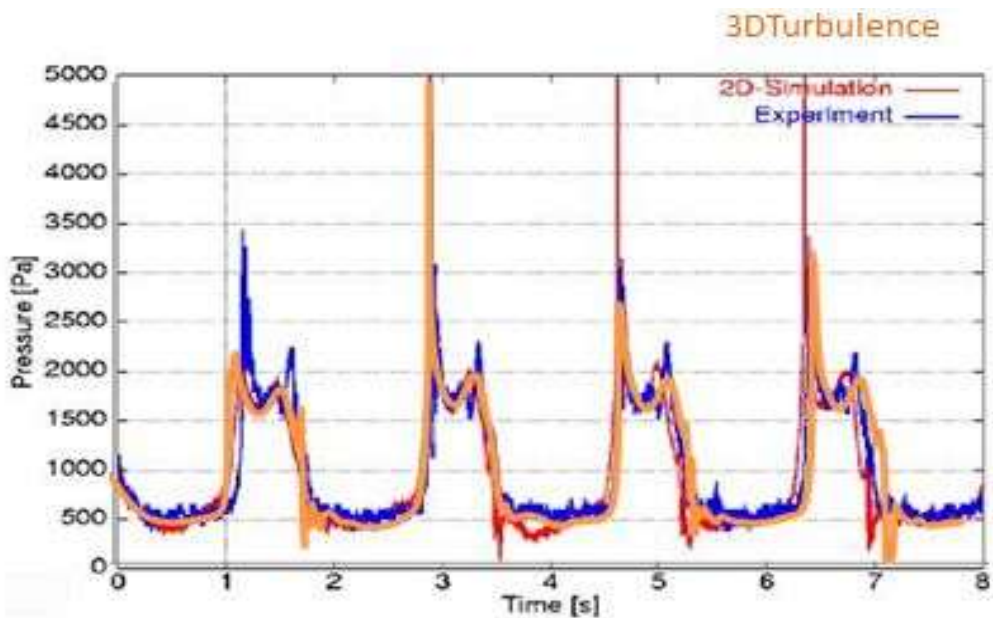


Figure 4.8: Comparison of simulated pressure time series (symbols) to experimental data of Hinatsu et al.[8] for $A=60$ mm, $T=1.74$ second, for P2 for 3D case

Figure 4.7 shows comparison between mine STARCCM+ and Hinatsu et al [8]work for 2D at the beginning of the simulation, due to the initial movement of the tank, water accelerates First cycle is removed because of weak sloshing. From Second cycle there is increase in pressure then there is sudden drop in pressure and then gradual increase in pressure . In all cycle STARCCM+ follows exactly same pattern as Hinatsu et al [8] result. In all cycle one it is clear that first peak is higher than second peak this is because in first peak liquid is hitting to the north wall and then liquid slightly return back so that every time second peak is lower. The maximum pressure is reaching till 5000 pa.

Figure 4.8 shows comparison between mine STARCCM+ and Hinatsu et al [8]work for 3D case. In this case time chosen 1E-03.The measure feature is same here also. Simulations started with the fluid being initially at rest. During the first oscillation period, the free surface is smoothed practically two-dimensional. However, in the second period the waves start overturning and breaking, and the liquid splashes on side walls, reaching in some cases the ceiling. From then onwards, the free surface becomes highly three dimensional. The only difference is that it shows similar result to the experimental set up result.

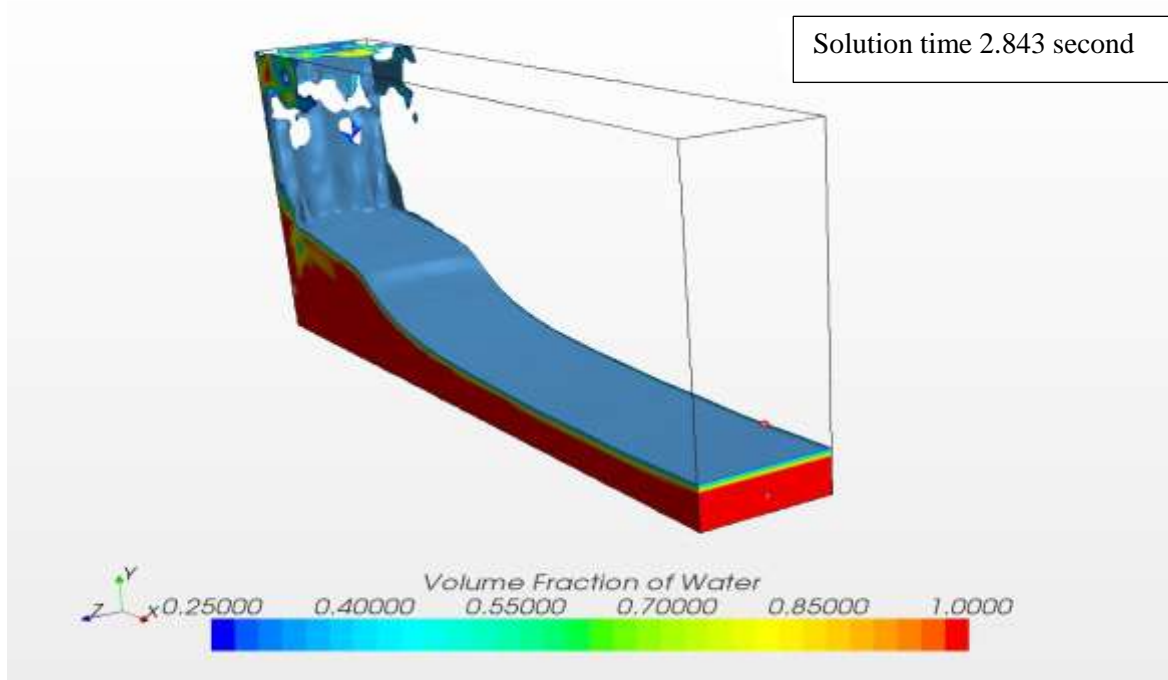


Figure 4.9: Sloshing during 2.843 second

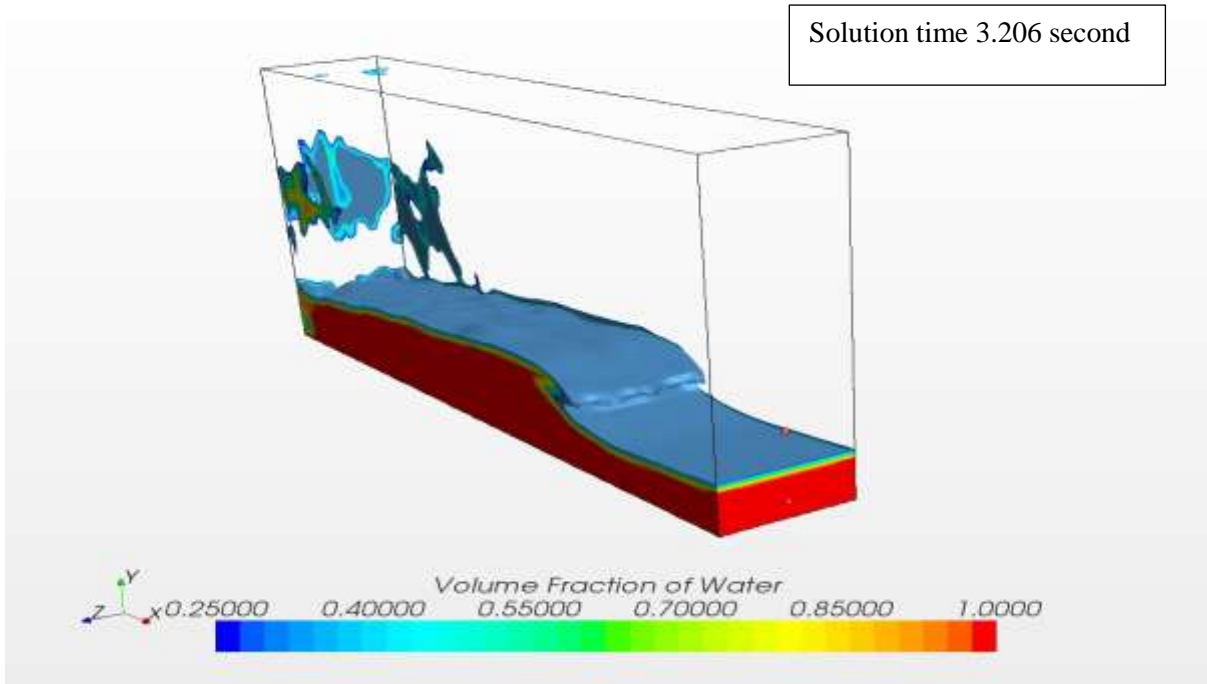


Figure 4.10: sloshing on during solution time 3.206 second

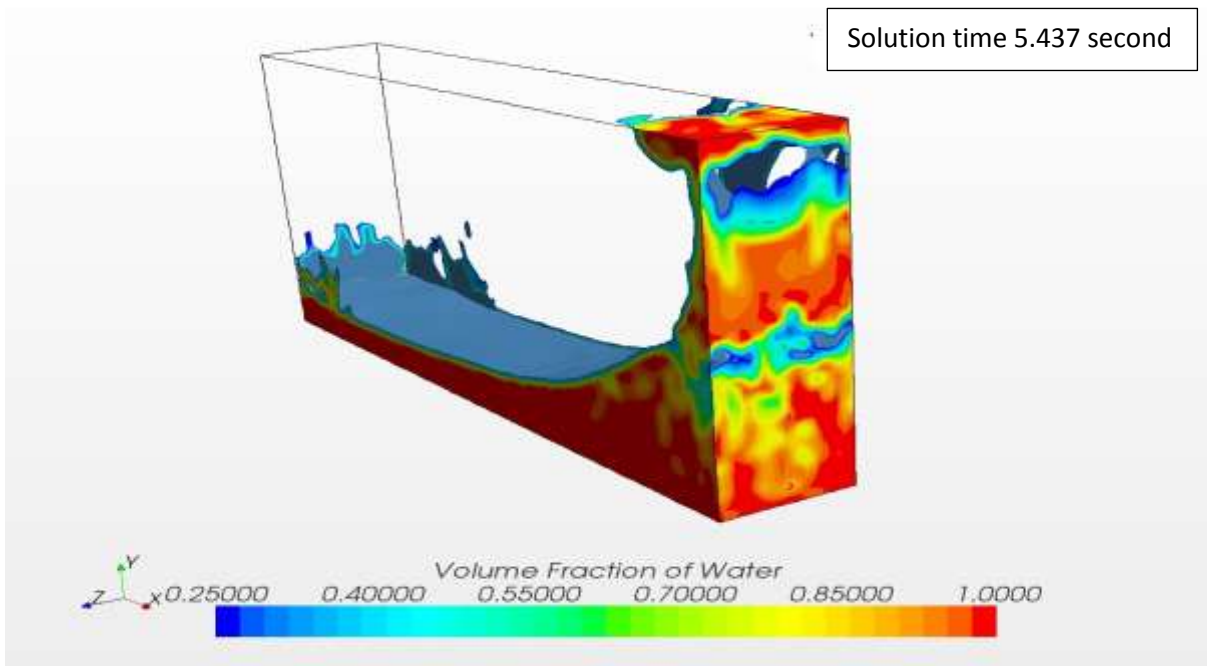


Figure 4.11: sloshing on during solution time 5.437 second

Figure 4.8, Figure 4.9, Figure 4.10 shows free-surface shapes he period of 1.74 s and a 3D simulation. This is near to resonance case in which liquid keeps hitting the ceiling as it is accelerated up the side walls, and both 3D and 2D simulations predict this phenomenon correctly.

4.4 Viscous effect

As discussed on previous section that there is no significant different in result either model is chosen turbulence or laminar. In this section simulation run for all three model turbulence, laminar and in viscous and all three are predicting similar result. There are following similar pattern.

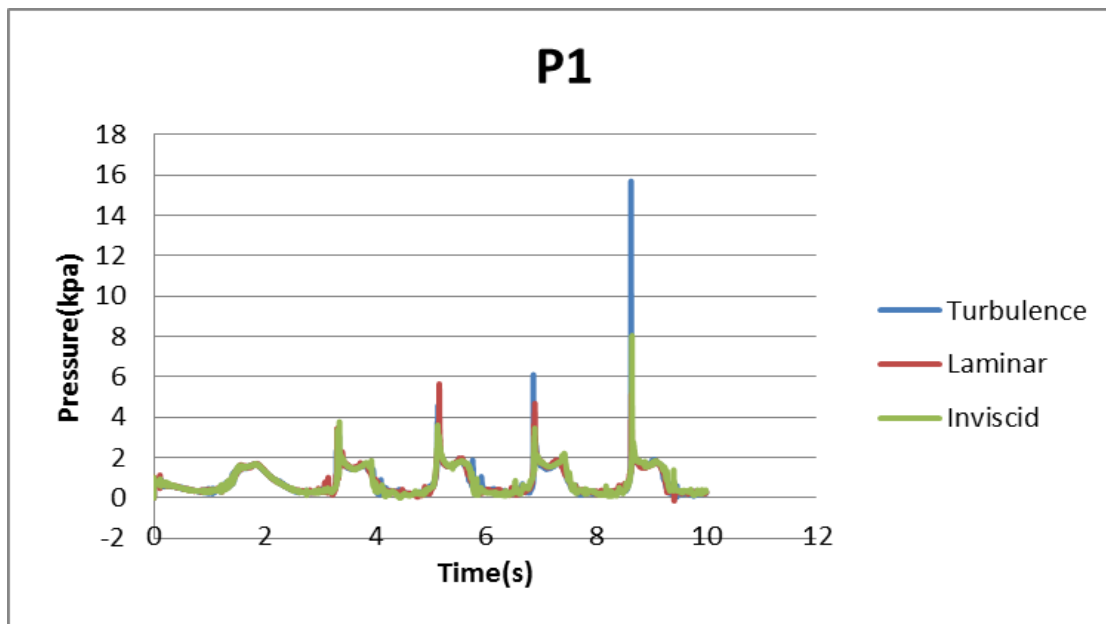


Figure 4.11: Viscous effect on P1

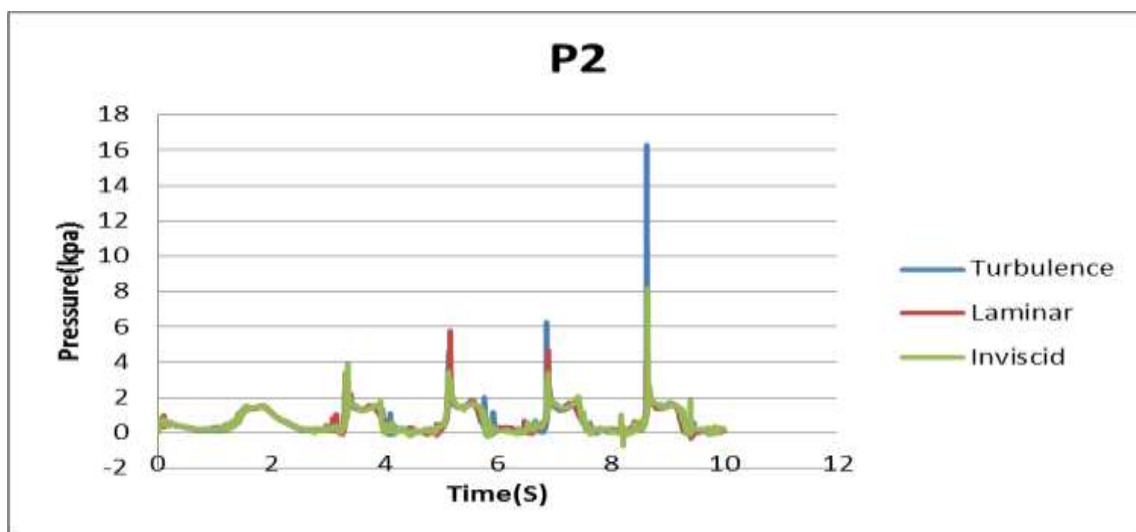


Figure 4.12: Viscous effect on P2

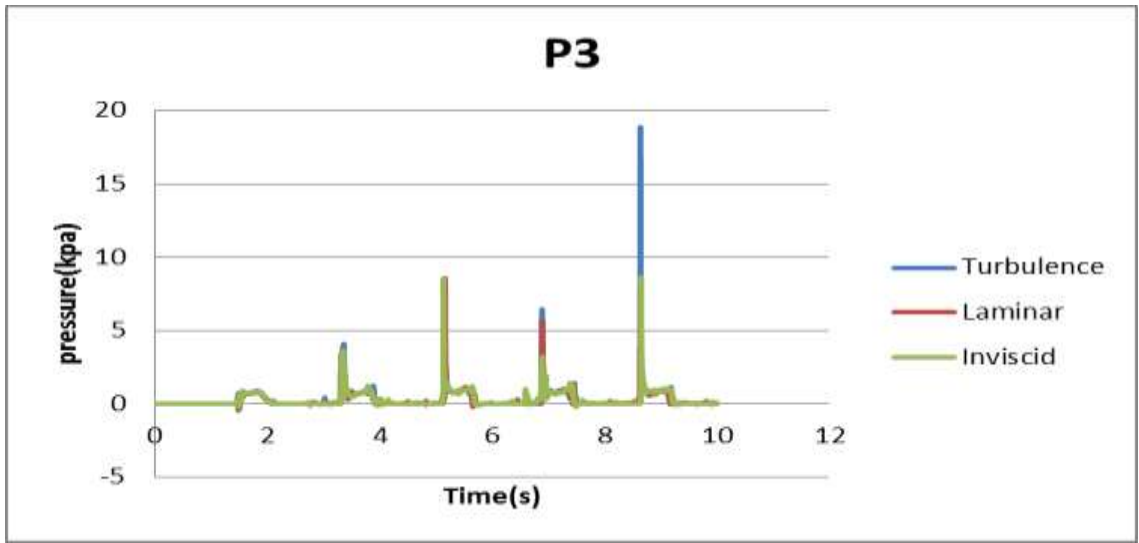


Figure 4.13: Viscous effect on P3

As figure shows Figure 4.11, Figure 4.12 and Figure 4.13 all three model follow same pressure variation .In turbulence the at last peaks are high and peaks for in viscid the peaks are less compare to laminar and turbulence. Using turbulence model it takes more time compare to laminar and in viscid because turbulence solve two more equation compare to laminar and in viscid.

4.5 Parametric study

There is various parametric study have been done like effect of fill ration, effect time period and effect of amplitude.

4.5.1.Effect of fill level

To study the effect of fill ration simulation run for filling level of 10%,20%,40% and 80%

	Water level(%)	T(s)	A(mm)
Case 1	10	1.74	60
Case 2	20	1.74	60
Case 3	40	1.74	60
Case 4	80	1.74	60

Table 4.1: Effect of fill level

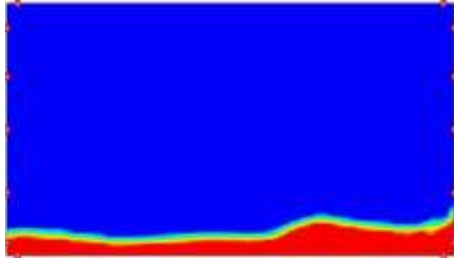


Figure 4.14(a): 10%

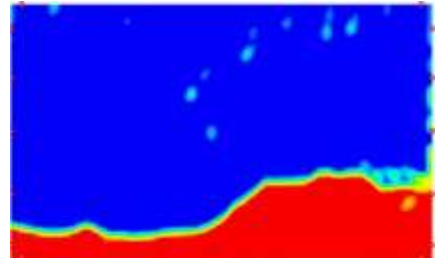


Figure 4.14(b): 20%

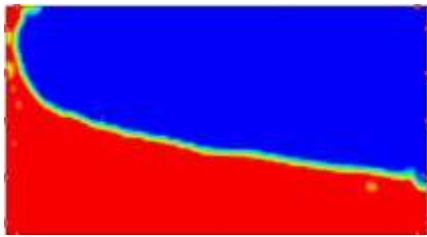


Figure 4.14(c): 40%

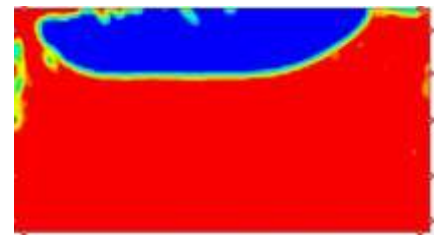


Figure 4.14(d): 80%

Figure 4.14: Fill ration at 7.395 second

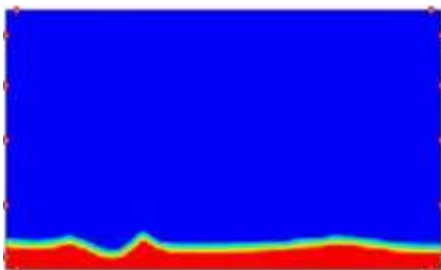


Figure 4.15 (a): 10%

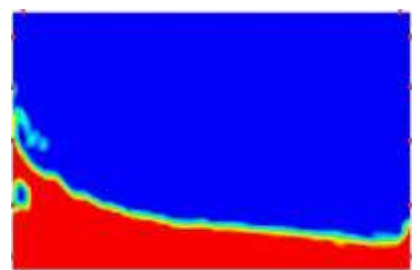


Figure 4.15(b): 20%

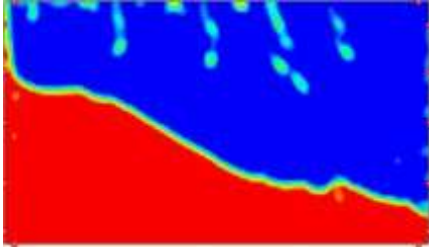


Figure 4.15(c) : 40%

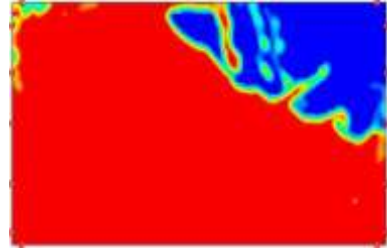


Figure 4.15(d):80%

Figure 4.15: Fill ratio at 7.83 second

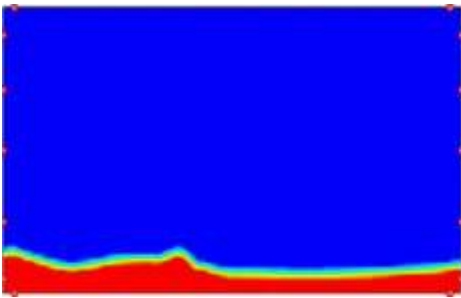


Figure 4.16(a): 10%

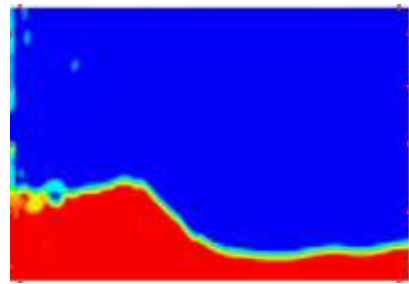


Figure 4.16(b): 20%

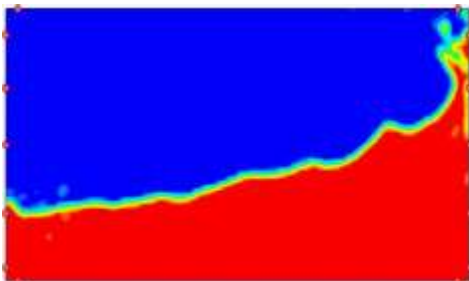


Figure 4.16(c):40%

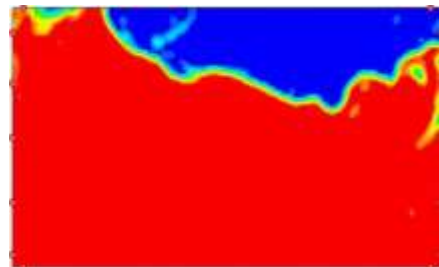


Figure 4.16(d) :80%

Figure 4.16: Fill ration at time 8.265 second

Figure 4.14 shows variation of fill ration on fourth cycle at various solution time. At solution time 7.395 second it is observed that for 10% and 20% the liquid is showing same pattern but on 40% and 80% it shows that in a solution time mass of liquid is transfer to left wall and pattern of 40% and 80% liquid height is same.

Figure 4.15 shows variation of fill ration at solution time 7.83 second now in this case all are showing same pattern and liquid start hitting left wall. As the liquid level increase liquid also start hitting roof of the wall and pressure magnitude also increase.

Figure 4.16 shows variation of fill ration at solution time 8.265 second. Again same thing is happening is that 10% and 20% is showing similar pattern and 40% and 80% shows similar pattern.

4.5.2 Effect of time period

To find the effect of time period solution run for 1.16, 1.45, 1.74 and 5.22 time period. Figure 4.17 shows P2 plot for different time period

	Water level(%)	T(s)	A(mm)
Case 1	20	1.16	60
Case 2	20	1.45	60
Case 3	20	1.74	60
Case 4	20	5.22	60

Table 4.2: Effect of Time period

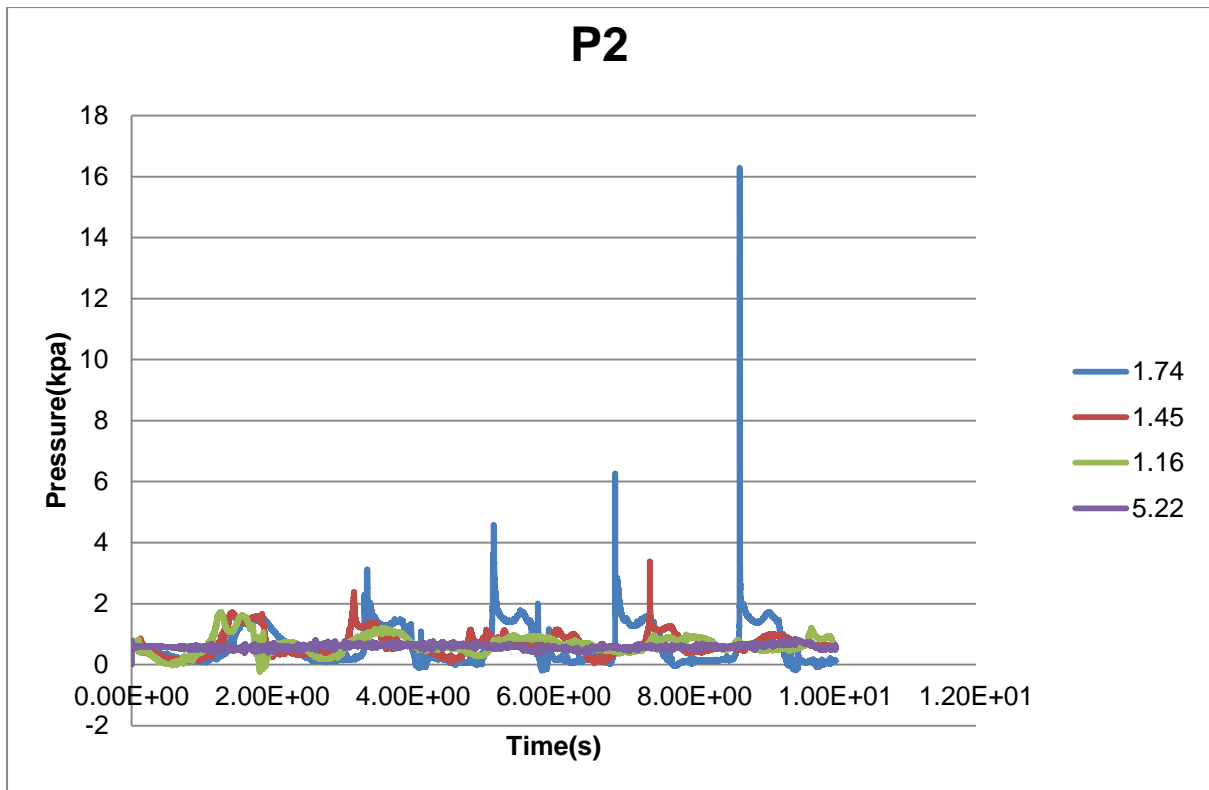


Figure 4.17: Effect of time period on P2

Figure 4.17 shows effect of time period on sloshing. It is clear that for a time period of 1.74 seconds, the pressure peaks are high because it is near to a resonance condition. In a resonance condition, sloshing is maximum. While for 5.22 seconds, there is no variation occurring because it is far from a resonance condition.

4.5.3 Effect of amplitude

Figure 4.18 shows the effect of amplitude on sloshing. The amplitude is varied from 30 mm to 120 mm in increments of 30 mm.

	Water level(%)	T(s)	A(mm)
Case 1	20	1.74	30
Case 2	20	1.74	60
Case 3	20	1.74	90
Case 4	20	1.74	120

Table 4.3: Effect of amplitude

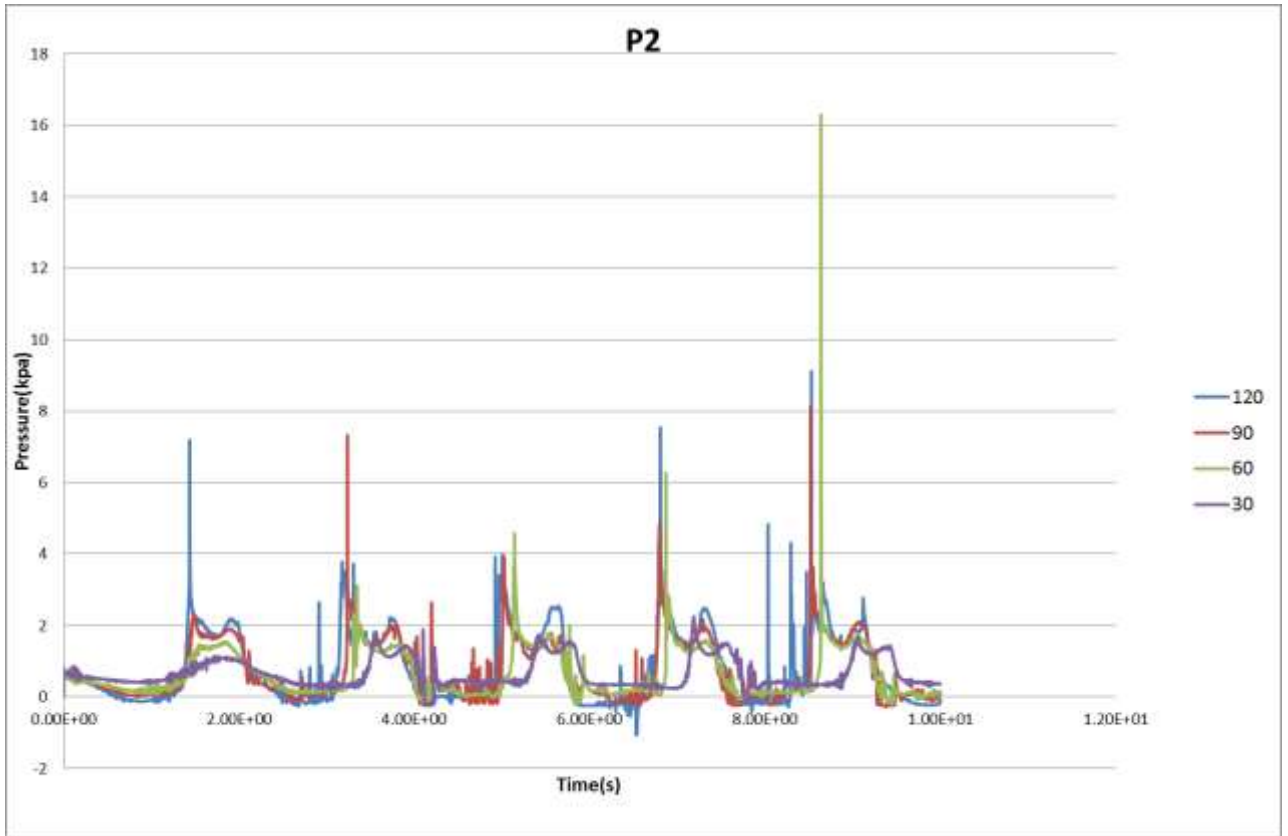


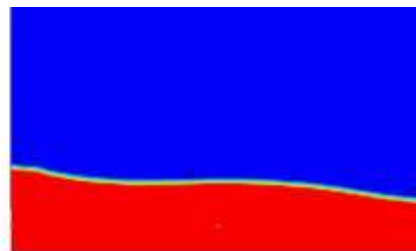
Figure 4.18: Effect of amplitude

4.6 Validation from experiment

In this section validation from experiment has been done. There is flow visualization has been shown between experimental and simulation result. Dimension of tank is $(23.8 \times 22 \times 23.8\text{cm})$. In experiment flow visualization has captured by high speed camera



Experimental

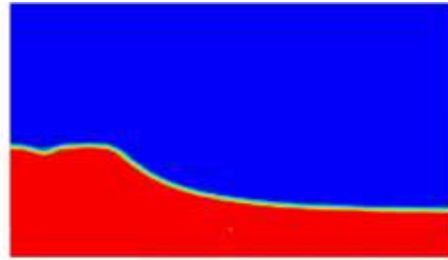


CFD

Figure 4.19(a): Flow visualization at 1.6387 second



Experimental

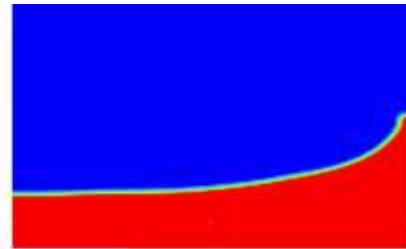


CFD

Figure 4.19(b): Time 2.3286 second



Experiments



CFD

Figure 4.19(c) : Time 4.72264 second

There is one experiment with 25% water levels and dead weight required to start tank motion were conducted. The aim of the experiment was to (i) measure the distance travelled by the tank over time using a proximity sensor and (ii) visualize the fluid motion before and after impact. Figure 4.19(a), Figure 4.19(b), Figure 4.19(c) shows a typical raw data for a 25% water level driven by a dead weight. The output signals were obtained from the proximity sensor from which the tank displacement and elapsed time can be obtained. Figure 4.19(a), Figure 4.19(b) and Figure 4.19(c) the sloshing after applying brake in the tank. Figure 4.19(a) and Figure 4.19(b) shows that bulk of fluid moved toward left and hit the left wall. Figure 4.19(c) fluid level at 4.72264 second. Figure 4.19(d) shows that now liquid moving and hitting the right wall. The experimental profiles compare well with the CFD results; both show the build up against the right, left then right – wall again of the fluid. But there is still some differences between CFD and experiments result the reason we have to figure out. The wave height of fluid is measured at different location of tank and the percentage of error is shown in below table-

s.no.	Cfd: wave height	Exp : wave height	%
1	0.31	0.411	24.57
2	0.257	0.253	-1.58
3	0.17	0.089	-91.0

Table 4.4(a): Wave height at 1.63867 second

s.no.	Cfd: wave height	Exp : wave height	%
1	0.387	0.466	16.95
2	0.366	0.46	20.43
3	0.387	0.466	16.95
4	0.15	0.03	-400

Table 4.4 (b) :Wave height at 2.3286 second

s.no.	Cfd: wave height	Exp : wave height	%
1	0.202	0.16	-26.25
2	0.238	0.204	-16.66
3	0.306	0.266	-15.03
4	0.494	0.511	3.32

Table 4.4(c): Wave height at 4.72264 second

Chapter 5

Conclusion

5.1 conclusions from simulation

5.1.1. CFD grid

The grid independence study has been discussed was discussed on *chapter 4* to establish in the validity of the results irrespective of any grid used. Other motions can now be studied using the selected grids with a reasonable degree of confidence of having used a suitable grid. It must be emphasized that including a third spatial dimension would make the current problem essentially a four dimensional one, implying a prohibitive increase in computational times. So that 128 grid is best for present problem.

5.1.2. Time step

For present problem simulation run for many time step like $1E-3, 1E-4, 1E-05$. It found that if time step is large second peak in pressure get vanished and also if the time step is very small it will just only increase the computational time. So that it concluded that $1E-4$ time step is suitable for present numerical case. It is also found that temporal discretization should be second order. Time step is controlled by courant number. So that if grid is refined the time step should be also refined.

5.1.3. Laminar or Turbulent Flow

In line with the calculated Reynolds number it was found that the flow is appropriate for turbulence modeling. The pressure histories obtained with a turbulence model showed two transient phases followed by a transition to the steady state. Using turbulence model more fluctuation is visible it also increase the computational time. For turbulence $k-\epsilon$ turbulence used and it gives good result.

5.1.4. 2D or 3D

For sloshing the simulation should run 2D or 3D. both 2D and 3D predict same qualitative variation is variation. 3D exactly shows result similar to experimental while 2D shows different result compare to 3D result in terms of peaks height . For saving computational time simulation should be running 2D only

5.2 Parametric study conclusion

5.2.1 Effect of fill ration

Simulation run for 10%, 20% ,40%, 80%. It is also found that higher peaks occurs at 20% and 80% of water of level. It is also observe that roof impacts are seen for fill levels of 50% and above.

5.2.2 Effect of time period

Simulation run for time period of 1.16 second,1.45 second,1.74 second and 5.22 second. It is found that time period 1.74 second is is very close to resonance frequency so that sloshing is maximum in this case. For 5.22 time period sloshing is very weak because it is far away from resonance condition.

5.2.2 Effect of Amplitude

Present sloshing case run for 30mm,60mm,90mm,120mm amplitude cases. It is found that Increasing the amplitude of sway increases the sloshing height of the water in the tank. For the higher amplitudes, the water can be seen to hit the roof at one instant and leave the bottom of the tank dry at another instant in time. Further increases in amplitude do not serve to increase the pressure further.

5.3 Conclusion from CFD and experiments

The water sloshing phenomenon in a rectangular tank under sudden impact was investigated experimentally and numerically There is comparison has been has done between experiment set up in IITH and STARCCM+ simulation and it is flow visualization of both result showing good agreement but there is significant variation in wave height which should be figure out in future.

5.4 Future work

5.4.1 Measure noise- I developed CFD methodology to predict slosh noise. In future using another commercial software slosh noise will be predicting using CFD pressure data.

5.4.2 Measure pressure data and noise for experimental set up- There pressure and noise will be measure for experimental set up and that result will be validating using commercial software.

5.4.3.Work on actual fuel tank – In future investigation of pressure and noise should be done Actual fuel tank of automobile.

References

- [1] Olsen H. What is sloshing 1976. In Seminar on liquid sloshing. Det Norske Veritas.
- [2] Hakan Akyildiz, Erdem Unal. 2005 “Experimental investigation of pressure distribution on a rectangular tank due to the liquid sloshing”, *Ocean Engineering* 32 (2005) 1503–1516.
- [3] Bernhard Godderidge, Mingyi Tan¹ Stephen Turnock¹ Chris Ear².2006 “A Verification and Validation Study of the Application of Computational Fluid Dynamic the Modeling of Lateral Sloshing” *Fluid Structure Interaction Research Group Ship Science Report No 140*.
- [4] Abramson, H.N., 1996. The dynamic behavior of liquid in moving containers. Report SP 106 of NASA. Boo, S.Y., 2002. Linear and nonlinear irregular waves and forces in a numerical tank. *Ocean Engineering* 29,475–493.
- [5] L. Khezzar, A. C. Seibi & A. Goharzade” *Water Sloshing in Rectangular Tanks – An Experimental Investigation & Numerical Simulation”* Petroleum Institute Abu Dhabi,UAE.
- [6] Hamid Rezaei, Mohammad Javad Ketabdari.2007 “Numerical Modeling of Sloshing with VOF Method” *The 12th International Conference on Fluidization - New Horizons in Fluidization Engineering*.
- [7] Milovan Perić Tobias Zorn.2005 “SIMULATION OF SLOSHING LOADS ON MOVING TANKS” *24th International Conference on Offshore Mechanics and Arctic Engineering, Halkidiki, Greece*.
- [8]Hinatsu, M., Tsukada, Y., Fukusawa, R. and Tanaka, Y., (2001) ‘Experiments of two-phase flows for the joint research’, In proceedings of SRI-TUHH mini-Workshop on Numerical Simulation of Two-Phase Flows, edited by M. Hinatsu, pages 12-19, National Maritime Research Institute, Tokyo, Japan
- [9] K.P. Thiagarajan D.Rakshit,N.Repalle.2011 “The air–water sloshing problem: Fundamental analysis and parametric studies on excitation and fill levels” *Ocean Engineering* 38 (2011) 498–508.
- [10] Lin Hou¹, Fangcheng Li¹ and Chunliang Wu².2012 “A Numerical Study of Liquid Sloshing in a Two-dimensional Tank under External Excitations” *J. Marine Sci. Appl.* (2012) 11: 305-310.
- [11] C.Z. Wang, B.C. Khoo .2004 “Finite element analysis of two-dimensional nonlinear

sloshing problems in random excitations “Ocean Engineering 32 (2005) 107–133.
and Eng., 88, 17-74.

[12] Stefan aus der Wiesche, 2006 “Noise due to sloshing within automotive fuel tanks”, *Forsch Ingenieurwes*, vol. 70, pp. 13-24.

[13] C. Wachowski¹, J.-W. Biermann¹, R. Schala “Approaches to analyse and predict slosh noise of vehicle fuel tanks”

[14] Hirt, C.W. and Nichols, B.D., 1981 ‘Volume of Fluid (VOF) method for the dynamics of free boundaries’, *Journal of Computational Physics*, 39, 201-225.

[15] Price, W.G., Chen, Y.G., 2006. A simulation of free surface waves for incompressible two phase flows using a curvilinear level set formulation. *Int. J. Numer. Methods Fluids* 51, 305–330

[16] El Moctar, O., 2006. Assessment of sloshing loads for tankers. *Shipp. World Shipbuild.* 204, 28–31

[17] Rhee, S.,H., 2005. Unstructured grid based Reynolds-Averaged Navier–Stokes method for liquid tank sloshing. *J. Fluids Eng.* 127 (3), 572–582

[18] Standing, R.G., Amaratunga, S., Lopez-Calleja, F., Orme, S., Eichaker, R., 2003. Marine hydrodynamics modeling using CFD. In: *Proc. Comput. Fluid Dyn. Technol. Ship Hydrodyn.* (CFD 2003), 1–12 London.